

Tunable high-power fiber laser and its application to produce Brillouin fiber lasers

**By
Jonas Kestutis Valiunas**

A thesis submitted to the faculty of graduate studies
Lakehead University
In partial fulfillment of the requirements for the degree of
Master of Science in Physics

Department of Physics
Lakehead University
March 2011
© Jonas K. Valiunas

Lakehead

UNIVERSITY

OFFICE OF GRADUATE STUDIES

NAME OF STUDENT: Jonas Kestutis Valiunas

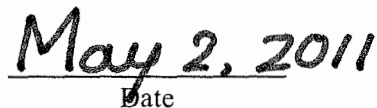
DEGREE AWARDED: Master of Science

ACADEMIC UNIT: Physics

TITLE OF THESIS: Tunable high-power fiber laser and its application to
produce Brillouin fiber lasers

This thesis has been prepared
under my supervision
and the candidate has complied
with the Master's regulations.


Signature of Supervisor


Date

Abstract

A tunable continuous wave single-longitudinal-mode fiber laser is proposed and developed. A saturable absorber, as well as, an all-fiber Fabry-Perot filter was used in the laser cavity to reduce mode-hopping. The laser was tunable from 1565nm to 1575nm and could produce an output power of 300mW while still maintaining single-mode operation with no mode-hopping. The linewidth of the laser was ~ 9 MHz. The stability of the laser based on the length of the saturable absorber and the modal structure has been explored. We developed two Brillouin fiber lasers using this laser as a pump source. A highly nonlinear photonic crystal fiber and a chalcogenide fiber were used as the nonlinear medium. The Brillouin fiber laser based on PCF could produce either single wavelength or multiwavelength laser outputs. Further, we investigated the coupling mechanism for the pump light into the chalcogenide glass fiber. In all cases the lasers were operated at room temperature.

Acknowledgement

I would like to thank all of my family and friends who have supported and helped to keep me motivated while completing my degree. I would especially like to express my appreciation for my supervisor, Dr. Gautam Das, who not only has been a great mentor, immensely supportive, and helpful, but who has also become a good friend. The countless hours he has dedicated to assisting and supporting me throughout my studies have been invaluable. I would also like to thank; Zachari Medendorp, for his direction, advice, and friendship; Zachary Chaboyer for his help, advice, and enjoyable company; Jean-Marc Lachaine, Kristine Carey, my supervisory committee (Dr. Mark Gallagher and Dr. Apichart Linhananta), and the entire Lakehead University Physics faculty who have essentially taught me everything I know about physics.

This thesis is dedicated to my mother, Dorothy,
and to my twin sister, Julia.

Contents

Abstract.....	II
Acknowledgements.....	III
List of Figures.....	VI
List of Tables.....	VII

Chapter 1

Introduction

1.1 Introduction.....	1
1.2 Optical Fibers.....	1
1.2.1 Single-mode Fiber	
1.2.2 Multimode Fiber	
1.2.3 Gain Fiber	
1.2.4 Polarization Maintaining Fiber	
1.2.5 Specialty Fibers	
1.3 Fiber Lasers.....	6
1.4 Theory.....	8
1.4.1 Brillouin Scattering	
1.4.2 Raman Scattering	
1.5 Brillouin Fiber Laser.....	12
1.6 Organization of the Thesis.....	12
References.....	14

Chapter 2

High Power Fiber Laser

2.1 Introduction.....	16
2.2 Experimental Setup.....	18
2.2.1 Double Clad Erbium-Ytterbium Co-doped Fiber (DC-EYDF)	
2.2.2 Tunable Fiber Bragg Grating	
2.2.3 Saturable Absorber	
2.2.4 Polarization Controller	

2.2.5 Optical Isolator	
2.2.6 Fiber Couplers	
2.2.7 All-Fiber Fabry-Perot Filter	
2.3 Results and Analysis	31
2.4 Discussion and Summary	43
References	45

Chapter 3

Brillouin Fiber Laser by Highly Nonlinear Photonic Crystal Fiber

3.1 Introduction	49
3.2 Experimental Setup	52
3.3 Results and Analysis	54
3.4 Discussion and Summary	58
References	59

Chapter 4

Brillouin Fiber Laser Based on Chalcogenide Fiber

4.1 Introduction	61
4.2 Arsenic Selenum Fiber (As₂Se₃)	63
4.3 Experimental Setup and Discussions	66
4.4 Results and Analysis	70
4.5 Discussion and Summary	74
References	75
Future work	77

List of Figures

Figure 1.1	General structure of an optical fiber.....	2
Figure 1.2	Light coupling within and outside of the acceptance angle of a fiber.....	3
Figure 1.3	a) A double clad erbium/ytterbium co-doped fiber, b) erbium doped fiber, c) polarization maintaining erbium doped fiber.....	5
Figure 1.4	a) a bowtie structured PMF, b) a PANDA PMF, c) an elliptical core PMF.....	5
Figure 1.5	Illustration of Brillouin scattering.....	10
Figure 1.6	Illustration of (a) Spontaneous Stokes Scattering, (b) Spontaneous Anti-Stokes Scattering and (c) is Second-order Spontaneous Stokes Scattering.....	12
Figure 2.1	Experimental setup of the fiber laser.....	17
Figure 2.2	Cross-sectional diagram of DC-EYDF used.....	20
Figure 2.3	Energy levels of ytterbium and erbium ions.....	21
Figure 2.4	Absorption and emission spectrum of the DC-EYDF (CorActive).....	21
Figure 2.5	Fiber Bragg Grating.....	22
Figure 2.6	A tunable Bragg grating system.....	22
Figure 2.7	Distribution of intensity along the length of the saturable absorber.....	24
Figure 2.8	Polarization controller setup.....	25
Figure 2.9	Propagation of light waves through the optical isolator in the allowed direction.....	27
Figure 2.10	Propagation of light waves through the optical isolator in the attenuated direction.....	27
Figure 2.11	Cross sectional diagram of fiber couplers.....	28
Figure 2.12	Schematic of all-fiber Fabry-Perot filter.....	29
Figure 2.13	Theoretical output of a ring resonator and Fabry-Perot filter.....	31
Figure 2.14	Output characteristics of the pump laser diode.....	31
Figure 2.15	Output of the MM fused fiber coupler.....	32
Figure 2.16	Output power of the laser at ~ 0.6 nm intervals from 1565nm – 1575nm.....	33
Figure 2.17	(a) Output of the laser obtained with OSA; (b) Input-Output characteristics of the laser without the SA for 1565.52 nm light.....	34
Figure 2.18	Output of the laser obtained using scanning Fabry-Perot spectrum analyzer.....	35
Figure 2.19	Output of the laser obtained using a power meter at a wavelength of 1565.52 nm.....	36
Figure 2.20	Output power of the laser with and without the saturable absorber.....	37
Figure 2.21	Output of the laser with the SA inside the cavity.....	38
Figure 2.22	Output of the laser when the laser operated in the pulsed regime.....	39
Figure 2.23	Output of the laser obtained from the oscilloscope.....	40
Figure 2.24	Output of the laser without the tunable fiber Bragg grating (TFBG).....	41

Figure 2.25	Output of the laser at different setting of the polarization controller. (a) Multiwavelength laser with wavelength separation of 0.22 nm; (b) Single wavelength laser.....	42
Figure 2.26	Output of the laser with tunable fiber Bragg grating (TFBG).....	43
Figure 3.1	a) The structure of a highly nonlinear solid core PCF, (b) a hollow core PCF fiber.....	50
Figure 3.2	Experimental setup of Brillouin ring cavity.....	51
Figure 3.3	Controlled collapse of PCF air holes when splicing to SMF, (a) a hole can be seen at SMF-PCF interface, (b) multiple arcs eliminated the hole.....	53
Figure 3.4	Output of the Brillouin fiber laser for an input pump power of 450 mW at 1565.96 nm wavelength, (a) Multiple scan at 2 minutes interval; (b) single scan.....	55
Figure 3.5	Output of the multiwavelength Brillouin fiber laser at different polarization controller plates position.....	56-57
Figure 4.1	Loss spectrum of the arsenic selenium fiber used (CorActive).....	63
Figure 4.2	Different misalignments that can occur when coupling fibers through free space techniques.....	68
Figure 4.3	The circuit diagram of the Brillouin fiber laser section.....	69
Figure 4.4	X-Position vs output power from the chalcogenide fiber for an input pump power of 1.18 mW.....	71
Figure 4.5	Output obtained from Optical Spectral Analyzer at different input powers: (a) 1.5 A (124mW) and (b) 3.0A (300 mW).....	72

List of Tables

Table 4.1	Important parameters for As ₂ Se ₃ and SiO ₂ fiber.....	65
-----------	--	----

Chapter 1

1.1 Introduction

Fiber lasers remain a very attractive area of research despite already being a mature technology, this is due to their useful properties including ease of maintenance, cost effectiveness, and high-quality diffraction-limited beams. Fiber lasers are no longer just the backbone of the telecommunication industry, but have found applications as pressure sensors in automobile bumpers[1], welding and cutting materials, and sensing of noxious gases [2;3].

The objective of the thesis is to develop a continuous wave laser and to investigate its interactions with highly nonlinear media. In this chapter we will briefly discuss the fundamentals of lasers, optical fibers, and nonlinear phenomena.

1.2 Optical Fibers

An optical fiber is a cylindrical dielectric waveguide designed for transmitting electromagnetic waves, and regularly made out of amorphous silica (SiO_2) [4]. They are typically very thin and flexible resulting in a highly durable waveguide that is resistive to

most chemicals at room temperature [5]. Advancements in fiber fabrication processes have resulted in extremely low loss silica based optical fiber (~ 0.2 dB/km).

There are many different types of optical fibers that are designed with specific characteristics like high nonlinearity, wider transmission bandwidth, or to maintain polarization. These characteristics are usually realized by altering the geometrical structure of the fiber core, changing the optical material [6], or both. Other materials used to make fibers are fluoride, phosphate, or chalcogenide glasses.

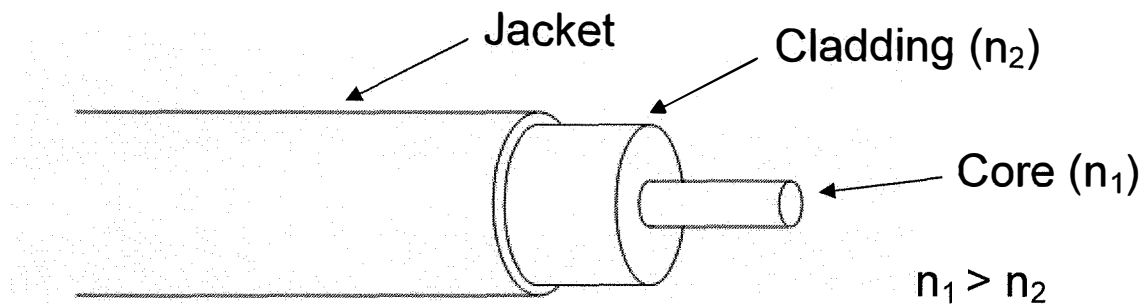


Figure 1.1: General structure of an optical fiber.

A typical optical fiber is composed of two silica (SiO_2) glass cylinders, one encompassed within the other as shown in Figure 1.1, where n_1 is the refractive index of the core and n_2 is the refractive index of the cladding. The index of refraction of the core is larger than that of the cladding, and the light is guided through the core by means of total internal reflection (Figure 1.2). Fibers are fabricated by first constructing a preform of the glass fiber structure. These are most commonly created by using the process of modified chemical vapor deposition (MCVD). MCVD is done by mixing SiCl_4 and O_2 vapors at 1800°C and depositing it on the inside of a silica tube. The tube is then heated so that it collapses in on itself and forms the preform [7]. The preform is then heated and

pulled into a fiber which is covered with a polymer coating. This coating reinforces the glass, making the fiber very durable.

In order for light to be guided within the fiber the radiation must be incident on the fiber at an angle which is within the acceptance angle. The acceptance angle is determined by the numerical aperture of the fiber [4].

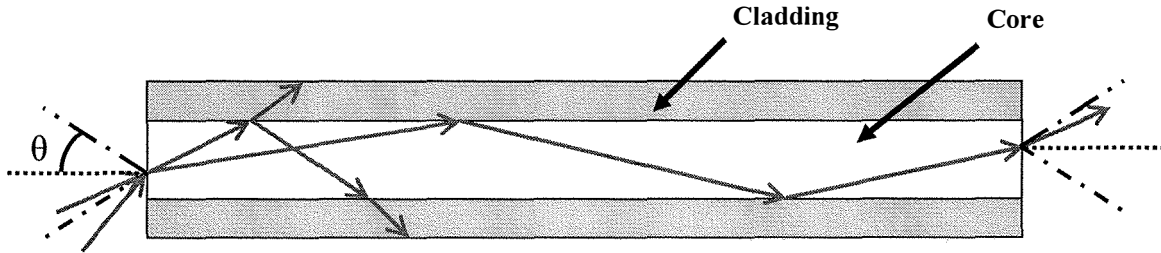


Figure 1.2: θ is the acceptance angle. Light entering the fiber core within the acceptance angle (green arrows) propagates through the core, while light entering at an angle greater than the acceptance angle (red arrows) propagates into the cladding and is lost inside the cladding.

Depending on the number of modes supported by an optical fiber one can have either a single-mode fiber (SMF) or a multimode fiber (MMF). A SMF can be used for developing passive and active optical components. The following subsections will briefly explain the structure of important fibers used in our experiments.

1.2.1 Single-mode Fiber

Single mode fibers support only one transverse mode and because of this they are free from intermodal dispersion. The general expression for determining the number of modes supported by an optical fiber is given as,

$$M \approx \frac{1}{2} \left(\frac{2\pi a}{\lambda} \right)^2 (n_1^2 - n_2^2) = \frac{V^2}{2} \quad (1.2)$$

where M is the number of modes, a is the core radius of the fiber, λ is the wavelength of the electromagnetic wave propagating through the fiber, n_1 and n_2 are the refractive indices of the core and cladding, respectively. A fiber is single mode if $V \leq 2.405$. A typical single mode fiber has a core diameter of 8-12 μm and a cladding diameter of 125 μm [4].

1.2.2 Multimode Fiber

A multimode fiber generally has a core diameter between 50-200 μm and a cladding diameter between 125-400 μm [4]. As its name implies, MMF supports many transverse modes. The fiber has large intermodal dispersion due to the presence of multiple modes and causes signal distortion. By using a graded refractive index fiber it is possible to reduce intermodal dispersion.

1.2.3 Gain Fiber

Gain fibers are essentially a regular optical fiber doped with a rare-earth element, such as erbium, ytterbium, neodymium, etc. These fibers can be utilized to develop active photonic devices such as amplifiers and lasers. Different methodologies have been developed to design gain fibers in recent years (Figure 1.3). A double-clad gain fiber was designed to allow large amounts of pump power to be efficiently coupled to the fiber and thus increase the conversion efficiency.

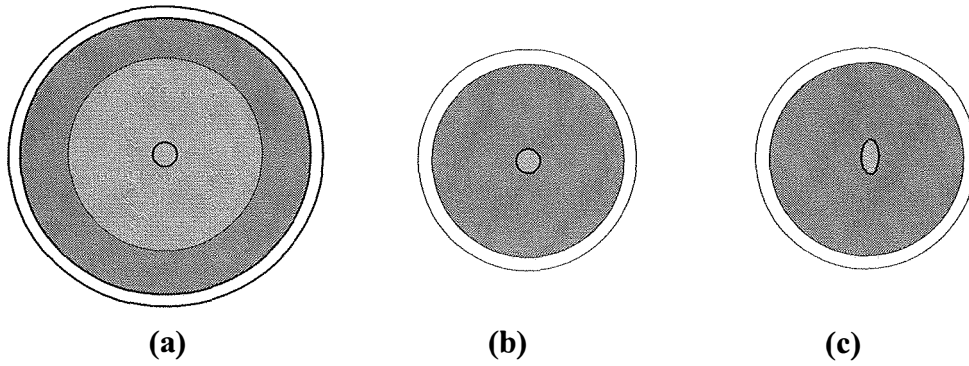


Figure 1.3: (a) A double clad erbium/ytterbium co-doped fiber, (b) erbium doped fiber, (c) polarization maintaining erbium doped fiber.

1.2.4 Polarization-Maintaining Fiber

Polarization is described as the direction in which the electric field of the propagating radiation is oscillating. A polarization-maintaining fiber preserves the polarization of the light inside the fiber. These fibers are designed to incorporate a birefringence throughout the fiber length, which can be done by either including a stress inducing material or by altering the geometrical shape of the fibers core. Figure 1.4 shows different types of polarization-maintaining fibers, where the shaded areas in figures (a) and (b) are stress inducing regions. Active fibers with polarization-maintaining properties and single or double cladding are commercially available.

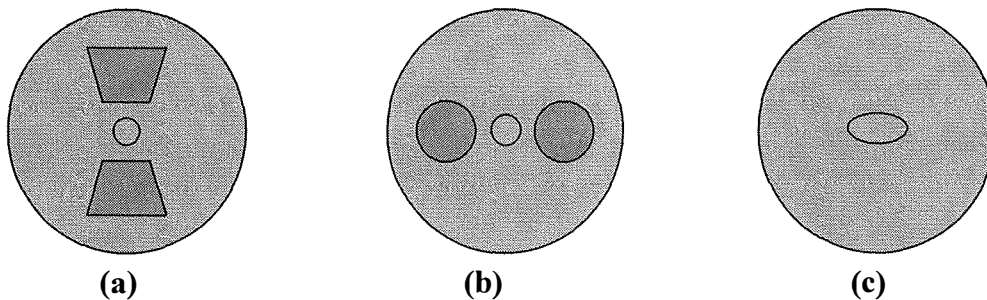


Figure 1.4: (a) a bowtie structured PMF, (b) a PANDA PMF, (c) an elliptical core PMF.

1.2.5 Specialty Fibers

In our experiments we used a Photonic Crystal Fiber (PCF) and a chalcogenide fiber as our nonlinear optical media. PCF fibers have found many applications for developing active and passive optical components. Signal waves propagate through the PCF by either following the principle of total internal reflection or photonic bandgap effects [8]. In Chapter 3, a more detailed explanation of PCF is given.

A Chalcogenide glass fiber is made from chalcogen elements; sulfur, selenium, or tellurium. These fibers are desirable because of their nonlinear properties as well as their ability to transmit light in the MID-IR wavelength range. Chalcogenide glass fiber has applications in sensing, signal buffering and amplification. A detailed description of the fiber is given in Chapter 4.

1.3 Fiber Lasers

LASER is an acronym for *Light Amplification by Stimulated Emission of Radiation*. In its simplest form a laser consists of a gain medium between two mirrors which forms the resonant cavity. Lasing action occurs when population inversion is achieved [9]. The first publication on lasers was credited to Schawlow and Townes in 1958 [10].

A fiber laser uses an active fiber as a gain medium in the ring or Fabry-Perot cavity configuration [11]. They have wide applications in industry and medicine because of their unique characteristics such as an all-fiber design, compact size, cost-effectiveness in production and operation, and without re-alignment or external cooling. The gain medium in general is a silica fiber doped with a rare-earth element. Fiber lasers are established as robust and reliable devices. Depending on the output power produced by a

fiber laser, it can be divided into two categories: (a) Low power laser and (b) high power laser.

High power lasers have applications in optical communications, sensing, medical instruments, industrial processing, and nonlinear optics. The advancement of fiber technologies such as the fiber fabrication processes, pumping techniques, and commercial availability of high power pump diodes have assisted in the development of high power fiber lasers [12;13]. Most of the high power fiber lasers employ a double-clad active fiber as the gain fiber.

Fiber lasers can also be divided into single-mode and multi-mode categories, depending on the modal structure of the laser. A single-mode laser contains only one longitudinal-mode. Though higher output powers can be obtained with a multimode fiber laser, single-mode operation is desirable in communications and sensing. To produce high output power from a fiber laser one can use either a double-clad active fiber together with a high power pump or Master Oscillator Power Amplifier (MOPA) configuration [14]. Using an erbium-ytterbium co-doped phosphate gain fiber in a ring resonator configuration, N. Peyghambarian et al. reported a single-mode fiber laser with an output power of 1W at 1.5 μm [15]. An erbium-ytterbium co-doped fiber has also been used to produce a single-mode high power laser [11]. High-power fiber lasers using erbium-ytterbium co-doped fiber as the gain medium, which operate in the eye-safe (1.5 μm to 1.6 μm) spectral range, can now compete with traditional solid-state lasers. The applications of the high-power lasers to date have been limited due to a narrow tunable range, large linewidth of the lasing wavelengths, multi-longitudinal-mode oscillation, and complex design [15;16].

1.4 Theory

The propagation of light in an optical fiber can be described by the Equation below,

$$\bar{\nabla} \times \bar{\nabla} \times \bar{E}(r, t) = -\frac{1}{c^2} \frac{\partial^2 \bar{E}(r, t)}{\partial t^2} - \mu_0 \frac{\partial^2 \bar{P}(r, t)}{\partial t^2} \quad (1.3)$$

where E is the electric field, c is speed of light in free space, μ_0 is the free space permeability, and P is the induced electric polarization. When an intense beam of light propagates through an optical fiber several nonlinear processes arise. The expression of the induced polarization can be written as

$$\begin{aligned} \bar{P}(r, t) = \varepsilon_0 \left(\chi^{(1)} \cdot \bar{E}(r, t) + \chi^{(2)} : \bar{E}(r, t) \bar{E}(r, t) \right. \\ \left. + \chi^{(3)} : \bar{E}(r, t) \bar{E}(r, t) \bar{E}(r, t) + \dots \right) \end{aligned} \quad (1.4)$$

where ε_0 is permittivity of the medium in free space, $\chi^{(1)}$ is the first order susceptibility, representing the linear portion of the polarization, while the higher order terms represent all of the nonlinear phenomena which may occur. Due to the inversion symmetry of the tetrahedral structural unit of silica the second order susceptibility, $\chi^{(2)}$ is zero. The third-order term, $\chi^{(3)}$ is responsible for most of the nonlinear effects in optical fibers, such as third-harmonic generation, four-wave mixing and nonlinear refraction. Since it is difficult to achieve the phase matching condition required for third-harmonic generation and four-wave mixing these two nonlinear phenomena do not readily occur in optical fiber.

The induced polarization (P) has two components, linear and nonlinear polarization, where the nonlinear term contains only the third order term (Equation 1.4), as shown below [7]

$$\vec{P}(r, t) = \vec{P}_L(r, t) + \vec{P}_{NL}(r, t) \quad (1.5)$$

Using the following relations

$$\vec{\nabla} \cdot \vec{D}(r, t) = \epsilon \vec{\nabla} \cdot \vec{E}(r, t) = 0$$

and

$$\vec{\nabla} \times \vec{\nabla} \times \vec{E}(r, t) = \vec{\nabla}(\vec{\nabla} \cdot \vec{E}(r, t)) - \vec{\nabla}^2 \vec{E}(r, t) = -\vec{\nabla}^2 \vec{E}(r, t) \quad (1.6)$$

one can reduce Equation 1.4 to the Scalar Wave Equation (Equation 1.7), which can be solved to find characteristics parameters of optical fibers.

$$\vec{\nabla}^2 \vec{E}(r, \omega) + n^2(\omega) \frac{\omega^2}{c^2} \vec{E}(r, \omega) = 0 \quad (1.7)$$

In the thesis we will investigate the nonlinear inelastic scattering phenomena known as Stimulated Brillouin Scattering (SBS) and Stimulated Raman Scattering (SRS). The nonlinear effects due to the third order nonlinearity are inelastic in nature. The nonlinear effects which arise due to stimulated inelastic scattering (SRS and SBS) are very important in optical fibers [7]. However, the main focus will be on stimulated Brillouin scattering. The fiber material, effective cross sectional area, effective fiber length, and input power all contribute to SBS and SRS. When a high intensity light beam propagates through an optical fiber the refractive index of the core will change according to:

$$\tilde{n}(\omega, |\vec{E}|^2) = n(\omega) + n_2 |\vec{E}|^2 \quad (1.8)$$

where $n(\omega)$ is the linear portion, $|\vec{E}|^2$ is the optical intensity inside the fiber and n_2 is the nonlinear constant related to the third order nonlinearity. The intensity dependent refractive index leads to two well known nonlinear effects; Self-Phase Modulation (SPM) and Cross-Phase Modulation (CPM).

1.4.1 Brillouin Scattering

Stimulated Brillouin Scattering can occur in an optical fiber at low input power with a narrow linewidth laser beam. An incident pump field inside an optical fiber generates an acoustic wave through the process of electrostriction, which modulates the index of refraction [17]. The pump-induced acoustic grating in the fiber causes the pump light to be scattered off of the moving acoustic wave at a slightly longer wavelength (Figure 1.5). This scattered wave is known as a Stokes wave. Once the input pump power reaches a threshold power the Stokes waves begin to increase exponentially.

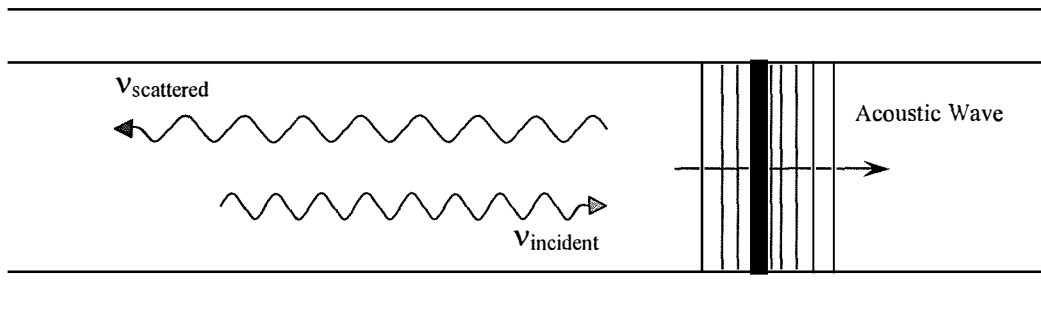


Figure 1.5: Stokes Brillouin Scattering. The incident frequency, ν_{incident} , is downshifted to the scattered frequency, $\nu_{\text{scattered}}$, after reflecting off of the moving acoustic wave, this is due to the Doppler Effect.

Stimulated Brillouin Scattering (SBS) is much easier to achieve and maintain in materials which have long phonon lifetimes. The decay rate is equal to the inverse of the phonon lifetime,

$$\Gamma_B = \frac{1}{\tau_B} \quad (1.9)$$

and the Brillouin linewidth is directly proportional to the inverse phonon lifetime,

$$\Delta\nu_B = \frac{\Gamma_B}{2\pi} \quad (1.10)$$

1.4.2 Raman Scattering

Raman scattering occurs when incident light excites a molecule to a virtual energy level, emits a photon of lower energy than the incident one, and then decays to its initial state by radiating an optical phonon. This Raman Effect is referred to as Stokes scattering (Figure 1.6b). Anti-Stokes scattering occurs when the molecule is already in an excited state and the incident light excites it further. When the molecule decays it decays to an energy level below that of which it started, resulting in a photon being emitted with a greater energy than the incident one (Figure 1.6c).

Stimulated Raman Scattering occurs when the pump power exceeds a threshold power. The photons generated due to spontaneous Raman scattering get amplified as they propagate along the fiber with the incident pump beam. However, the frequency which has maximum Raman gain coefficient will build up rapidly. This is called Stokes frequency and is downshifted from the pump frequency by an amount dependent on the medium (13.2 THz for silica glass fiber)[7].

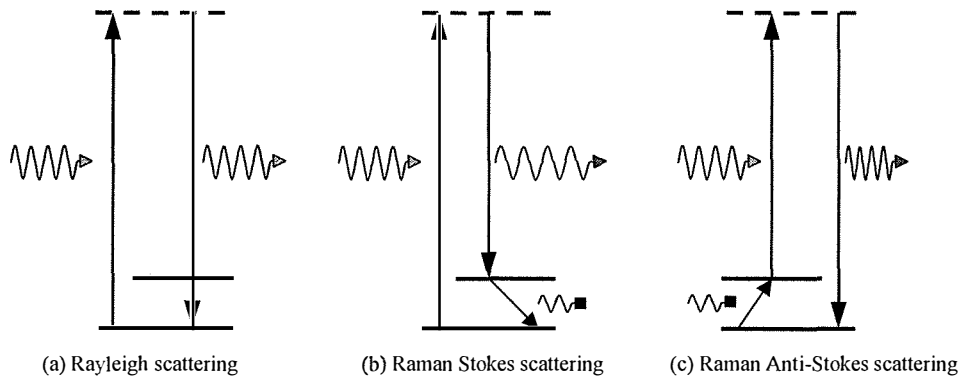


Figure 1.6: Illustration of (a) Spontaneous Stokes Scattering, (b) Spontaneous Anti-Stokes Scattering and (c) is Second-order Spontaneous Stokes Scattering.

1.5 Brillouin Fiber Laser

Though stimulated Brillouin scattering can be detrimental, it has some beneficial aspects. For instance, Brillouin scattered radiation has a very narrow linewidth which is very desirable for some sensing applications. Other novel applications outside of signal amplification and sensing are signal buffering and acoustic gratings. For example, Z. Zhang et al. theoretically presented a new buffering technique where they used acoustic waves created by SBS to delay the optical signal by many nanoseconds with little signal loss [18]. Nonlinear optical switching has been shown in a chalcogenide (As_2Se_3) glass fiber using long period gratings created by acoustic waves [19].

1.6 Organization of the Thesis

Chapter 2 describes the design of a high power fiber laser. The output power of the laser was more than 600 mW. The effect of a saturable absorber inside the laser resonator on the linewidth, stability, and output power has been explored. Further, we have investigated the condition for CW and pulsed operation and the condition for single-mode

and multi-mode oscillation of the laser. Finally, the laser was used to produce nonlinear effects in optical fibers based on different materials. Chapter 3 focuses on stimulated Brillouin scattering in a highly nonlinear photonic crystal fiber. We analyze the characteristics of the Brillouin laser output, such as linewidth, power and stability. We also discuss how we select either multi-wavelength or single-wavelength output by adjustments of the polarization controller and the effect of the elliptical core PCF in the system. Chapter 4 focuses on our experimentation with a chalcogenide fiber as a nonlinear medium for producing stimulated Brillouin scattering. We discuss a method for coupling light into the chalcogenide fiber and we compared our results with those reported in literature. The future work section presents ideas for future study or applications of our laser and nonlinear fiber.

References

- [1] P. Meyrueis, B. Kress, and S. Fischer, "Smart automotive bumper based on a multimode optical fiber," *Proceedings of SPIE: Photonics in the Transportation Industry: Auto to Aerospace*, vol. **6758**, no. Vision & Lighting Systems 2007.
- [2] D. G. Lancaster, D. Richter, and F. K. Tittel, "Portable fiber-coupled diode-laser-based sensor for multiple trace gas detection," *Applied Physics B-Lasers and Optics*, vol. 69, no. 5-6, pp. 459-465, Nov.1999.
- [3] S. T. Persijn, A. K. Y. Ngai, and F. J. M. Harren, "Fast-Scanning Fibre-Amplified Diode Laser Pumped cw OPO for Sensitive, Multi-Component Trace Gas Detection," 2007.
- [4] G. Keiser, *Optical Fiber Communications*, 3 ed. Boston, MA: McGraw Hill, 2000.
- [5] N.S.Kapany, *Fiber Optics: Principles and Applications* Academic Press Inc., 1967.
- [6] R. Mossadegh, J. S. Sanghera, D. Schaafsma, B. J. Cole, V. Q. Nguyen, P. E. Miklos, and I. D. Aggarwal, "Fabrication of single-mode chalcogenide optical fiber," *Journal of Lightwave Technology*, vol. 16, no. 2, pp. 214-217, Feb.1998.
- [7] G. P. Agrawal, *Nonlinear Fiber Optics*, 3rd ed Academic Press, 2001.
- [8] J. C. Knight, T. A. Birks, P. St. J. Russell, and D. M. Atikin, "All-silica single-mode optical fiber with photonic crystal cladding," *Optics Lett.*, vol. 21, no. 19, pp. 1547-1549, 1996.
- [9] A. E. Siegman, *Lasers* University Science Books, 1986.
- [10] A. L. Schawlow and C. H. Townes, "Infrared and Optical Masers," 112 ed 1958, pp. 1940-1949.
- [11] G. Das and Z. J. Chaboyer, "Single-wavelength fiber laser with 250 mW output power at 1.57 μm ," *Optics Express*, vol. 17, no. 10, pp. 7750-7755, 2009.
- [12] J. Nilsson, J. K. Sahu, Y. Jeong, W. A. Clarkson, R. Selvas, A. B. Grudinin, and S.-U. Alam, "High power fiber lasers: New Developments," *Proceedings of SPIE: Advances in Fiber Devices*, vol. 4974, pp. 50-59, 2003.
- [13] Y. Jeong, J. K. Sahu, D. N. Payne, and J. Nilsson, "Ytterbium-doped large-core fiber laser with 1.36 kW continuous-wave output power," *Optics Express*, vol. 12, no. 25, pp. 6088-6092, Dec.2004.
- [14] C. Alegria, Y. Jeong, C. Codemard, J. K. Sahu, J. A. varez-Chavez, L. Fu, M. Ibsen, and J. Nilsson, "83-W single-frequency narrow-linewidth MOPA using large-core erbium-ytterbium co-doped fiber," *Ieee Photonics Technology Letters*, vol. 16, no. 8, pp. 1825-1827, Aug.2004.
- [15] A. Polynkin, P. Polynkin, M. Mansuripur, and N. Peyghambarian, "Single-frequency fiber ring laser with 1W output power at 1.5 μm ," *Optics Express*, vol. 13, no. 8, pp. 3179-3184, Apr.2005.
- [16] Y. Jeong, C. Alegria, J. K. Sahu, L. Fu, M. Ibsen, C. Codemard, M. R. Mokhtar, and J. Nilsson, "A 43-W C-band tunable narrow-linewidth erbium-ytterbium

- codoped large-core fiber laser," *Ieee Photonics Technology Letters*, vol. 16, no. 3, pp. 756-758, Mar.2004.
- [17] R. W. Boyd, *Nonlinear Optics* Academic Press, 1992.
- [18] Z. Y. Zhang, X. J. Zhou, R. Liang, Z. J. Qin, and Y. Liu, "Numerical investigation on buffer performance based on acoustic excitation by stimulated Brillouin scattering in an As₂Se₃ fiber," *Optics Communications*, vol. 282, no. 14, pp. 2746-2751, July2009.
- [19] H. C. Nguyen, D. I. Yeom, E. C. Magi, L. B. Fu, B. T. Kuhlmeiy, C. M. de Sterke, and B. J. Eggleton, "Nonlinear long-period gratings in As₂Se₃ chalcogenide fiber for all-optical switching," *Applied Physics Letters*, vol. 92, no. 10 Mar.2008.

Chapter 2

Tunable single-longitudinal-mode high-power fiber laser

2.1. Introduction

Fiber lasers are established as robust and reliable devices. They have wide applications in industry and medicine because of their unique characteristics such as all-fiber designs, compact size, cost-effective production and operation, and no need for re-alignment or external cooling. High-power single-wavelength and multiwavelength fiber lasers, in the infrared region of the electromagnetic spectrum, are very attractive for applications in optical communications, sensing, spectroscopy, biomedical instrumentation, and nonlinear optics. The continued progress in fiber pumping techniques, advanced fiber designs, and fabrication processes as well as the availability of high power pump diodes, have assisted in the development of high power fiber lasers [1-5]. Several fiber lasers have been designed for the purpose of sensing temperature and

strain [6-9], medical diagnostics [10-12], sensors based on optical nonlinearity [13;14] and industrial processing [15]. There are still opportunities to develop new optical devices based on fiber laser technology.

High-power fiber lasers using erbium-ytterbium co-doped fibers as the gain medium, which operates in the eye-safe ($1.5\ \mu\text{m}$ to $1.6\ \mu\text{m}$) spectral range, can now compete with traditional solid-state lasers. The applications of recently reported single-wavelength [16;17] and multiwavelength [18;19] high-power fiber lasers were limited due to large linewidth of the lasing wavelength, multi-longitudinal-mode oscillations, small tuning range and complex designs.

In this chapter a novel tunable, high-power, single-wavelength, single-longitudinal-mode, fiber ring laser is demonstrated. In the following sections we describe the experimental setup, output of the laser, and working principles of active and passive components inside the cavity. We also discuss the suitability of the laser for producing nonlinear effects in highly nonlinear optical fibers.

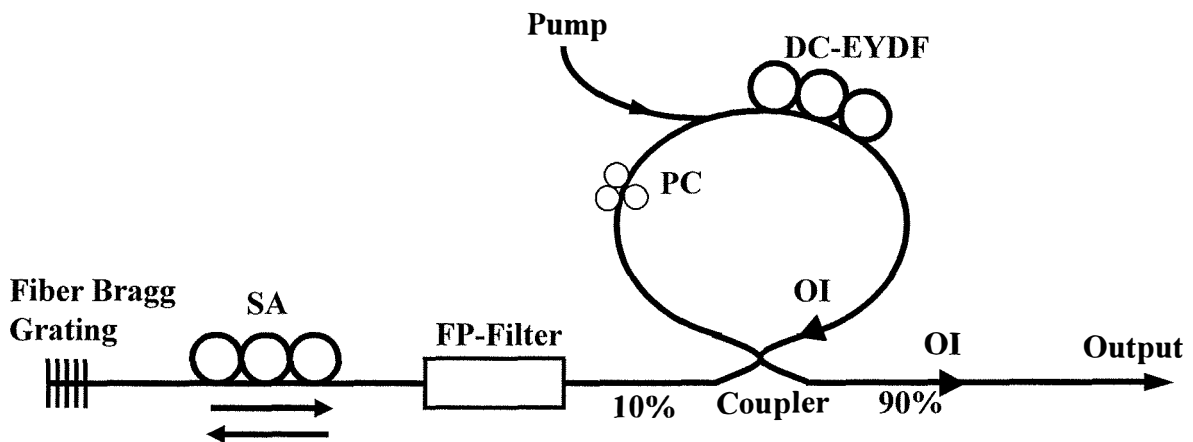


Figure 2.1: Experimental setup of the fiber laser.

2.2. Experimental Setup

Figure 2.1 shows the experimental setup of the fiber laser. The resonant cavity consists of a high-power polarization-independent optical isolator (OI), which guaranteed the unidirectional propagation of the waves inside the cavity, and thus eliminated spatial hole-burning effects [20]; an all fiber polarization controller (PC) to adjust the polarization of the light wave inside the cavity; a commercially available tunable fiber Bragg grating (TFBG) to select the lasing wavelengths, with a tuning range of over 10 nm (1565nm – 1575nm); a 4 m long double-clad erbium-ytterbium co-doped (DC-EYDF) fiber with core/cladding diameters of 10/131 μm was used as the gain medium. In general to produce high output power from a ring laser, a longer length of the active medium is required which leads to a smaller longitudinal-mode spacing and a narrower laser linewidth. A DC-EYDF with high conversion efficiency, as an active medium eliminated the requirement for a long length of the active medium. To increase the effective longitudinal-mode spacing and stability of the laser wavelength a Fabry-Perot filter (also known as etalon) with large free spectral range (FSR) was used inside the cavity. The all fiber Fabry-Perot filter was formed by splicing two 2×2 single-mode fused fiber couplers (split ratio 99:1) which eliminated mode hopping of the laser wavelength by increasing the effective longitudinal mode spacing of the laser cavity. An un-pumped polarization-maintaining (elliptical core) erbium-doped fiber (PM-EDF) was used as a saturable absorber (SA) inside the cavity to reduce the mode hopping of the lasing wavelength. A multimode fiber pigtailed 976 nm laser diode with a maximum output power of 10 W was used to pump the DC-EYDF. Due to the limitations of our fiber splicer we could not splice the multimode fiber pigtail into the circuit, thus we adopted a

free space coupling mechanism to couple the light from the pump laser into the cavity. A multimode fused fiber coupler (7×1 multimode pump power combiner) was used as a 976/1550 nm wavelength division multiplexing coupler to couple power from the pump laser diode into the DC-EYDF fiber. The fiber Bragg grating, saturable absorber, Fabry-Perot filter and the ring together formed an over-lapping cavity configuration, where the output of the ring resonator was modulated by the output of the Fabry-Perot cavity. The output of the laser was obtained from the 90% port of a 90:10 fused fiber coupler. A polarization independent optical isolator was used to reduce any back reflection from the output port. The output of the laser was monitored using an optical spectrum analyzer with a resolution of 1.25 GHz, a scanning Fabry-Perot spectrum analyzer (SFPSA) of resolution 6.7 MHz and a power meter. We investigated the effect of the saturable absorber on the lasers output power, modal structure, linewidth, and stability at room temperature.

The demonstrated laser was unique because of: i) the all fiber resonant cavity design; ii) application of commercially available tunable fiber Bragg grating (TFBG) to select and tune laser wavelengths; iii) use of an all fiber Fabry-Perot filter to increase longitudinal-mode spacing; iv) no active control unit was required to stabilize the laser; and v) moderate output power.

2. 2. 1. Double Clad Erbium-Ytterbium co-doped fiber (DC-EYDF)

The double clad geometry of the DC-EYDF allows high pump power radiation to be efficiently coupled to the active fiber which results in a large output power from the laser. The large surface area reduces the risk of damaging the fiber at high powers. The

core of the DC-EYDF fiber (Figure 2.2) is circular in shape and doped with erbium and ytterbium ions. The presence of ytterbium ions inside the erbium doped core reduces the clustering effects of the erbium ions, and also increases the coupling efficiency of the pump power [21;22]. A double-clad fiber with a hexagonal inner cladding was chosen because it has been shown to have a much greater absorption and coupling efficiency compared to that of a circularly symmetric double-clad fiber [23]. The inner cladding is surrounded by a second cladding which is comprised of silica and the entire fiber is covered in a protective jacket.

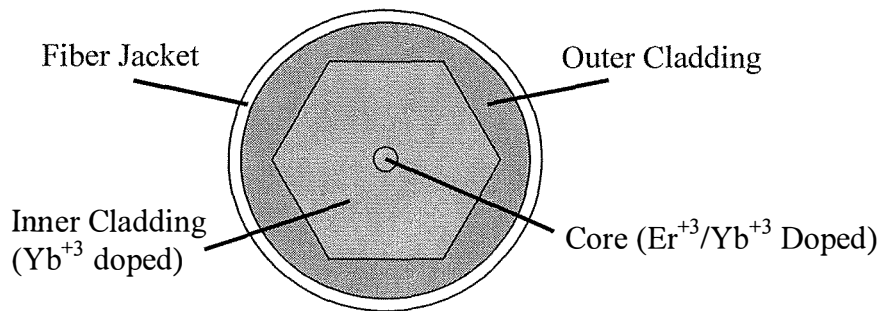


Figure 2.2: DC-EYDF fiber cross section.

Ytterbium ions have a large absorption cross-section and broader absorption band compared to that of the erbium ions. The pump power is first absorbed by the ytterbium ions and the energy is then transferred to the erbium ions non-radiatively by de-excitation of the ytterbium ions (Figure 2.3). This results in an increase in the spontaneous emission power of the laser oscillation and leads to higher output powers [24]. Figure 2.4 shows the absorption and emission spectrum of the DC-EYDF provided by the fiber supplier, CorActive, Canada. The ytterbium ions have their peak absorption at 976 nm. Due to the wider absorption band and geometry of the DC-EYDF, a multimode pump laser in the

800 nm – 1100 nm wavelength range can be used as the pump source. The large cladding diameter of the fiber can support many pump modes which increase the interaction between the ytterbium ions and pump radiation.

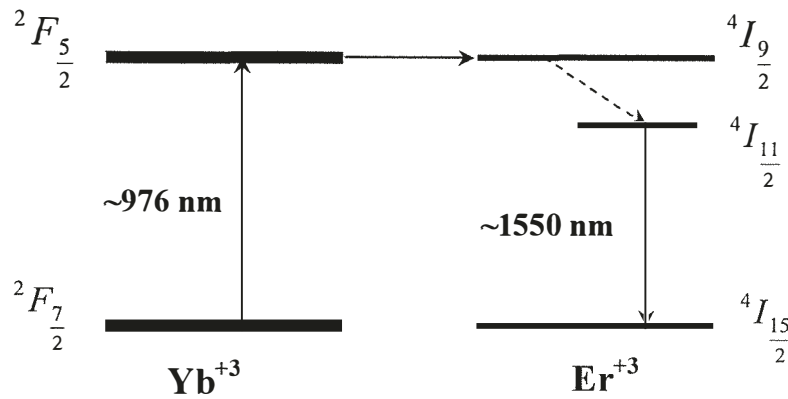


Figure 2.3: Energy levels of ytterbium and erbium ions.

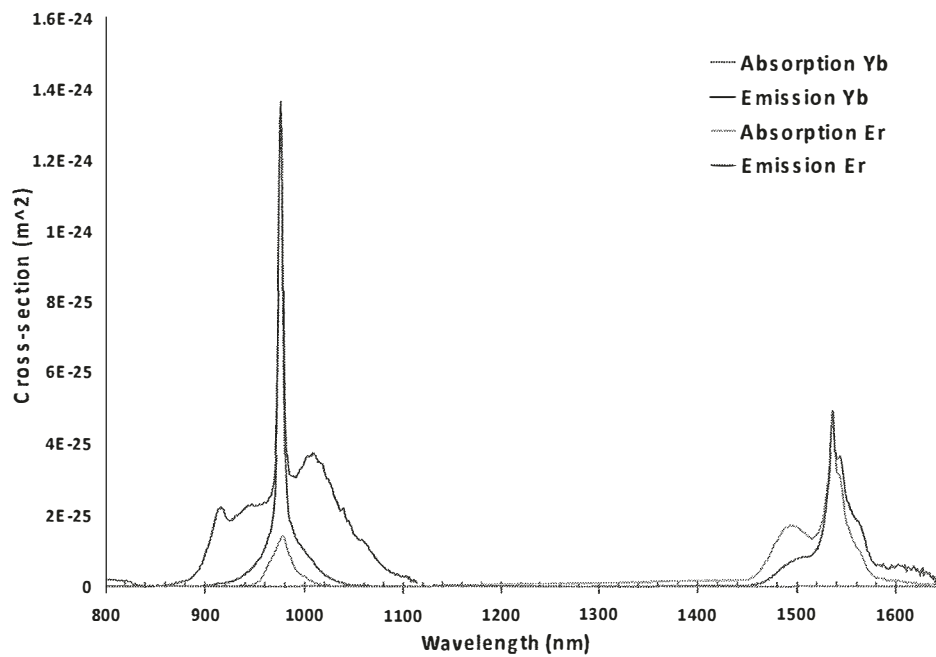


Figure 2.4: Absorption and emission spectrum of the DC-EYDF, CorActive.

2.2.2. Tunable Fiber Bragg Grating (TFBG)

A fiber Bragg grating (FBG) is formed by writing a periodic perturbation of the refractive index along the fiber core, and acts as a narrow band reflection filter (Figure 2.5). The maximum reflection occurs when the Bragg condition is satisfied and the corresponding reflected Bragg wavelength is given as [25]

$$\lambda_{Bragg} = 2n_{eff} \Lambda \quad (2.1)$$

where n_{eff} is the effective refractive index and Λ is the spatial period of the grating along the axis.

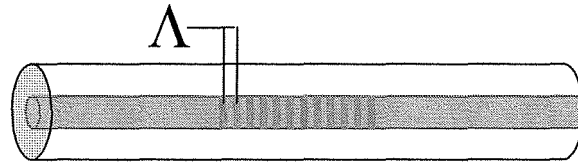


Figure 2.5: Fiber Bragg Grating.

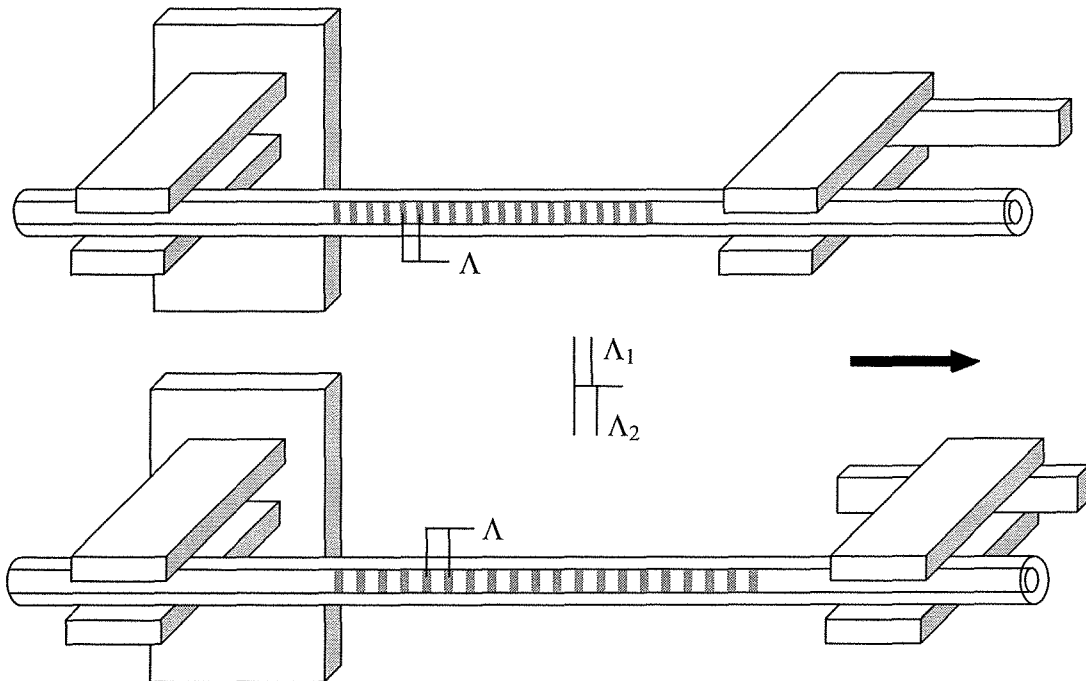


Figure 2.6: A tunable Bragg grating system.

A fiber Bragg grating is formed by placing a phase mask over the fiber with a period of Λ which corresponds to the desired reflected wavelength. The fiber is then exposed to UV light, which is passed through the mask on to the core. The radiation induces a change in the refractive index of the core at periodic intervals corresponding to the mask (Figure 2.5) and the reflected wavelength is determined by Equation (2.1). Any change in the grating such as stress or temperature, which varies modal index, spatial period, or both, will change the reflected wavelength.

A tunable fiber Bragg grating can be made by taking a regular FBG and placing it in a mechanism that can apply an adjustable stress to the entirety of the grating usually by pulling (Figure 2.6) or bending the grating [26].

2.2.3. Saturable Absorber (SA)

A saturable absorber (SA) is an optical material that exhibits an intensity dependent loss. An un-pumped, rare-earth (e.g. Er^{+3} , Sm^{+3}) doped optical fiber can be used as a saturable absorber. The effective loss in a laser cavity increases with longer length of SA and high rare-earth concentration. It is desirable to find a rare-earth doped fiber with an optimum length and rare-earth ion concentration to obtain a maximum output of the laser. The application of SA for passive Q-switched fiber laser is a very well known and established technique [27]. It has also been reported that a saturable absorber can be used inside a laser cavity to reduce the laser linewidth and mode hopping [28;29]. The counter propagating lightwaves inside the SA (Figure 2.1) interfere with each other and form a standing wave pattern. Figure 2.7 shows the periodic variation of light inside the SA. This periodic variation of light intensities modulates the refractive index of the fiber core

and thus induces a transient Bragg reflection grating. The strength, bandwidth and stability of the transient grating depends on the dopant concentration, the length of the saturable absorber, the intensity, and polarization states of the counter propagating light waves. The transient grating automatically adjusts itself for any change in the laser cavity. The general expression for the reflection bandwidth of the transient grating is [30;31]

$$\delta\nu = \frac{c}{2\pi n} \sqrt{\left(\frac{\pi}{L}\right)^2 + \frac{|k|^2}{1 + (\tilde{g}L/\pi)^2}} \quad (2.2)$$

$$\approx \frac{c}{2nL}$$

where n ($=1.46$) is the refractive index, k is the coupling coefficient, \tilde{g} is the saturated gain factor and L is the length of the saturable absorber. Equation (2.2) shows that the bandwidth of the transient grating is inversely proportional to the length of the saturable absorber. The SA that we used was a polarization-maintaining erbium doped fiber (PM-EDF) with core dimensions, peak absorption, cut-off wavelength and numerical aperture of $3.8 \times 14.8 \mu\text{m}$, 10.8dB/m at 1535nm , 1371 nm and 0.15 , respectively.

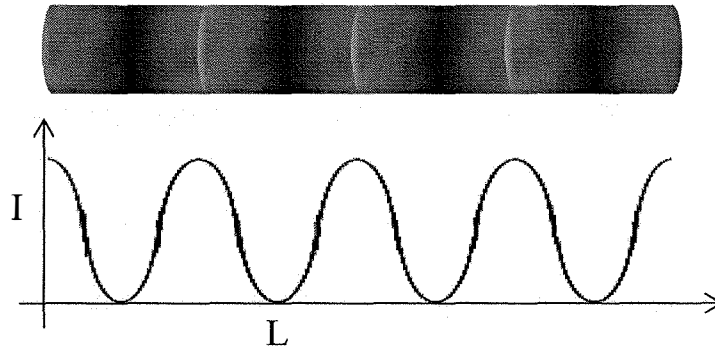


Figure 2.7: Distribution of intensity along the length of the saturable absorber.

2.2.4. Polarization Controller (PC)

The polarization controller (PC) plates are used to adjust the polarization state of the light inside the cavity. The polarization controller is formed by looping single mode fiber around three metal plates to form a configuration of a $\lambda/4$ wave plate, a $\lambda/2$ wave plate, and another $\lambda/4$ wave plate (Figure 2.8). In single mode fiber, birefringence occurs because of a deviation of the core geometry from the ideal straight circular cylinder. The bending induced birefringence of a single-mode fiber is given by

$$\Delta n = -C \left(\frac{r}{R} \right)^2 \quad (2.3)$$

where C (≈ 0.133) is a constant, r is the radius of the SMF, and R is the radius of the bend. By having a smaller bend radius we can produce a larger birefringence, however, bending a fiber also increases the attenuation which is why a very small radius is not practical.

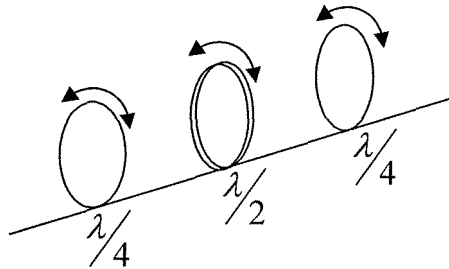


Figure 2.8: Polarization controller setup.

The amount of bend induced birefringence in an optical fiber is smaller than crystal birefringence, but the net effect is significant since it is accumulated along the fiber length. The bend induced phase difference between the two polarizations is:

$$\begin{aligned} \Delta\phi &= \frac{2\pi}{\lambda} \Delta n (2\pi RN) \\ &= \frac{4\pi^2}{\lambda} C \frac{r^2}{R} N \end{aligned} \quad (2.4)$$

where N is the number of turns of the fiber in a loop and λ is the wavelength of operation. We can achieve the effect of a wave plate by adjusting the number of loops made with the fiber. The fiber loops are free to rotate and a rotation of each loop will rotate the principle axes of the birefringent fiber sections with respect to the input polarization state. By rotating the PC plates it is possible to produce any polarization state. The two quarter wave plates control the ellipticity, and the half wave plate controls the orientation of the output polarization state [32].

2.2.5. Optical Isolator (OI)

The purpose of an optical isolator is to allow electromagnetic radiation to propagate in only one direction by attenuating light traveling in the opposite direction. In our experiment a polarization independent optical isolator was used to guarantee unidirectional wave propagation inside the cavity. The structure of an isolator is shown in Figure 2.9, where a Faraday rotator is placed in between two birefringent wedges. For incident light propagating in the allowed direction (as shown in Figure 2.9) through an optical isolator, the light is split into horizontal and vertical polarization states, by the birefringent wedge (1). The wedge possesses a fast axis and slow axis which causes the polarizations to spatially separate from each other. The light then enters into the Faraday rotator section, which rotates the polarization of the light by 45° . After which the light enters into the second birefringent wedge (2), which polarizes the light (horizontal and vertical) into -45° and 45° . The light which was polarized along the fast axis in wedge (1) is now polarized for the slow axis in wedge (2) and vice versa. Thus the two polarized states recombine at the output of the isolator and couple to the fiber.

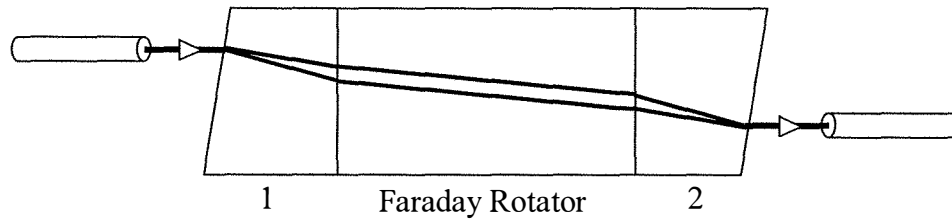


Figure 2.9: Forward propagating light waves through the optical isolator.

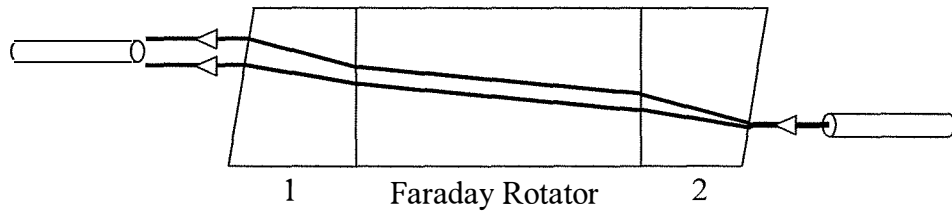
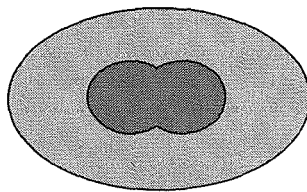


Figure 2.10: Backward propagating light waves through the optical isolator.

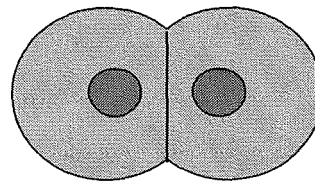
When the light travels in the opposite direction (Figure 2.10), the birefringent wedge (2) initially polarizes the light into -45° and 45° , once again the fast and slow axes cause the two different polarizations to spatially separate from each other. The light then enters into the Faraday rotator again and is rotated by 45° in the same direction it would be rotated if it was traveling in the forward direction (A Faraday rotator rotates the plane of polarization by 45° irrespective of the direction of propagation). The light that has traveled through the rotator will now be in vertical and horizontal polarized states. However, the light polarized for the fast axis in birefringent wedge (1) is the same light that was polarized for the fast axis birefringent wedge (2) which causes the light to spatially separate more. Since these two polarized light rays were separated twice they are not following the path which would couple them back into the core of the fiber and they become lost in the cladding of the fiber or are blocked by an aperture.

2.2.6. Fiber Couplers

A fiber coupler is a passive optical device widely used in telecommunications to divide or combine optical signals. A fiber coupler can have one or more input ports and one or more output ports (e.g. 2×2 coupler, $N \times N$ coupler- star coupler) depending on the application. Fiber couplers can be made to be either wavelength dependent or independent. A wavelength dependent coupler is used for wavelength division multiplexing in telecommunications, while a wavelength independent coupler is used as a combiner or splitter of optical signals. Among the different types of fiber couplers a fused biconical taper coupler is widely used in the optical communication industry. By using coupled mode theory one can design a fused fiber coupler with desired properties (e.g. coupling ratio). The detailed theory of the coupler is available in any standard Optical communication text book [33]. A fused fiber coupler is fabricated by twisting two fibers together, such that the regions forming the coupler are parallel, and then melting and pulling them to fuse the cores of the two fibers together (Figure 2.11a). Another method for producing a coupler is by polishing the sides of the fiber as shown in Figure 2.11b.



(a) Fused Fiber Coupler



(b) Polished Fiber Coupler

Figure 2.11: Cross section of fiber couplers.

2.2.7. All - fiber Fabry-Perot filter

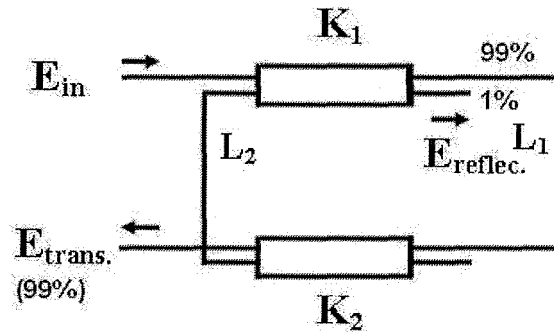


Figure 2.12: All-fiber Fabry-Perot filter, where K_1, K_2 are the coupling coefficients, L_1, L_2 are the lengths of the SMF, E_{in} , E_{trans} , and E_{reflec} are the incident, transmitted, and reflected electric fields, respectively [34].

The longitudinal-mode spacing of any fiber laser cavity is usually very small due to a long cavity length. The use of a Fabry-Perot (FP) filter is one of the techniques widely used to increase the longitudinal-mode spacing of a fiber laser cavity. The FP filter inside the cavity increases the stability of the laser by reducing mode hopping. In our design (Figure 2.1) an all-fiber filter was used to increase the longitudinal-mode spacing of the laser cavity [34]. The filter was formed by two fused fiber couplers (split ratio 99/1) as shown above in Figure 2.12. The expressions of transmitted and reflected electric fields are given below

$$\left. \begin{aligned}
 \frac{E_{trans}}{E_{in}} &= \frac{\sqrt{(1 - K_1)(1 - K_2)} \exp(J\beta L_{FP})}{1 + \sqrt{K_1 K_2} \exp(J\beta L_{FP})} \\
 \frac{E_{reflec}}{E_{in}} &= \frac{J(\sqrt{K_1} + \sqrt{K_2} \exp(J\beta L_{FP}))}{1 + \sqrt{K_1 K_2} \exp(J\beta L_{FP})}
 \end{aligned} \right\} \quad (2.5)$$

$$\left(\frac{E_{trans}}{E_{in}} \right)^2 + \left(\frac{E_{reflec}}{E_{in}} \right)^2 = 1$$

The separation between two transmission peaks or the free spectral range (FSR) of the Fabry-Perot filter is given by:

$$FSR_{FP} = \Delta \nu_{FP} = \frac{c}{nL_{FP}} \quad (2.6)$$

where c is the speed of light in free space, L_{FP} is the length of the cavity and n is the refractive index. In our experiment the length (L_{FP}) of the Fabry-Perot filter was $\approx 0.4\text{m}$, and the corresponding free spectral range was, $FSR_{FP} \approx 514\text{ MHz}$. The general expression for the FSR of a ring cavity resonator is determined by [35]

$$FSR_{Ring\ cavity} = \Delta \nu_{Ring\ cavity} = \frac{c}{nL_{eff}} \quad (2.7)$$

where L_{eff} is the effective cavity length. In general the length of the ring cavity is longer than the FP filter cavity, thus the presence of the filter inside the cavity produced the vernier effect (in Figure 2.13 transmission peaks of FP filter coincides with every tenth peak of the ring resonator) and increased the longitudinal-mode spacing of the cavity [36-38]. Figure 2.13 shows the typical output of a ring resonator together with a FP filter for an effective ring cavity of length 4m and a FP cavity length of 0.4 m [34]. It is clear from the Figure 2.13 that the presence of the FP filter increased the longitudinal mode spacing of the laser resonator cavity and thus reduced the mode hopping.

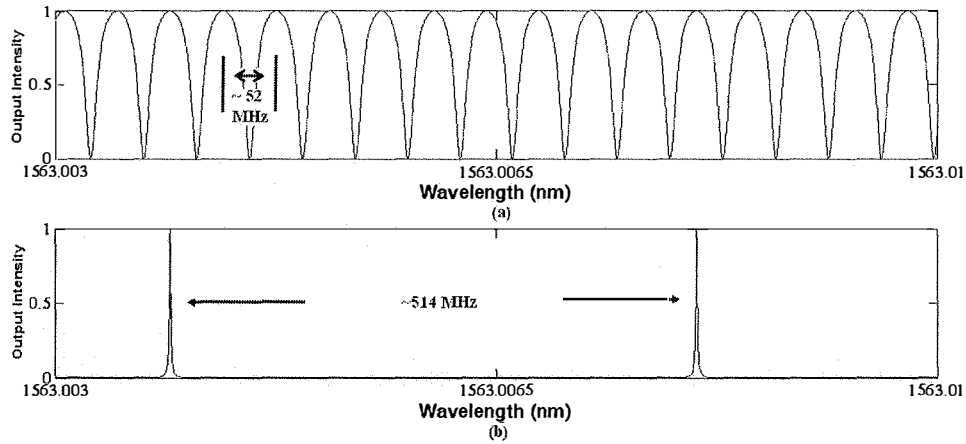


Figure 2.13: Theoretical output of a ring resonator and Fabry-Perot filter[34].

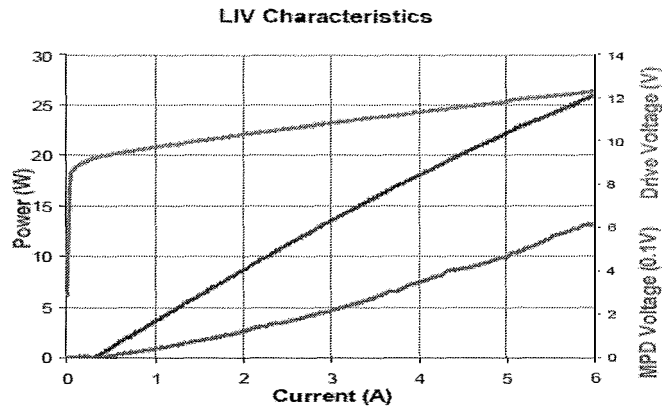


Figure 2.14: Output characteristics of the pump laser diode.

2.3. Results and Analysis

As stated earlier (Section 2.2.1) the active fiber of the laser was pumped by a high power multimode pigtailed laser diode. Figure 2.14 is the output characteristics of our pump laser as provided by the manufacturer. Figure 2.15 shows the power coupled into the laser cavity through the multimode fused fiber coupler which was measured with a power meter. It was found that only $\sim 30\%$ of the inputs pump power was used for pumping the active fiber.

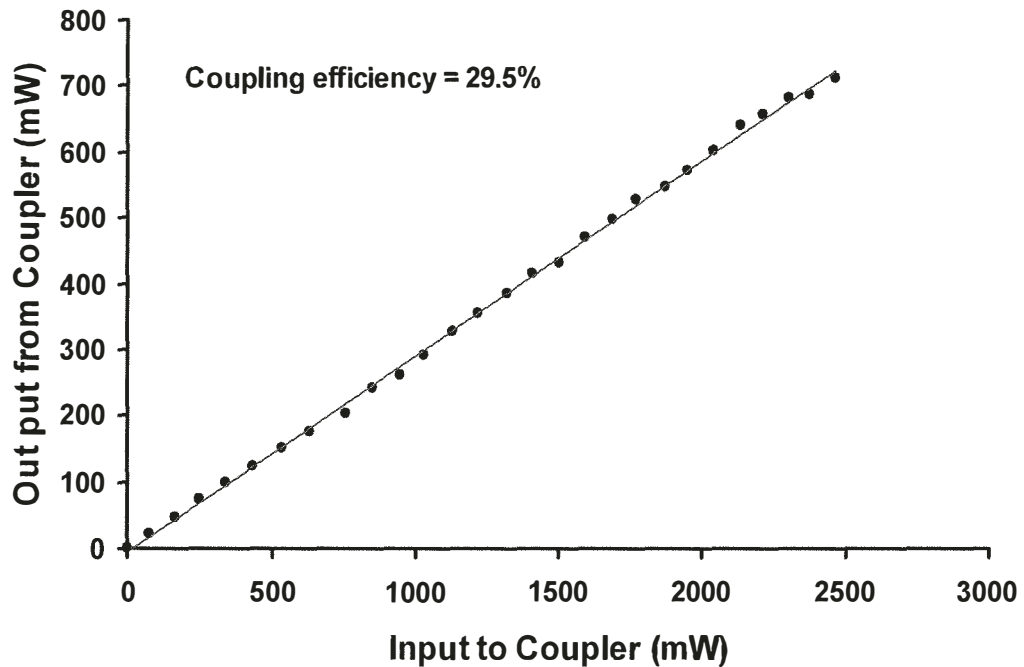


Figure 2.15: Output of the MM fused fiber coupler.

Figure 2.16 shows the tunable characteristics of the laser for an input pump power (coupled to the active fiber) of ~ 700 mW at a wavelength of 976 nm. The laser was tunable from 1565 nm – 1575 nm, which was limited by the tunability of the grating. The minimum tunable interval was 0.01 nm which was limited by the resolution of the optical spectrum analyzer. The non-uniform output power over the wavelength range is due to the erbium-ytterbium co-doped fiber emission, which decreases in this region (Figure 2.4). We operated the laser close to the ~ 1565 nm wavelength because the maximum output power was obtained in this wavelength region.

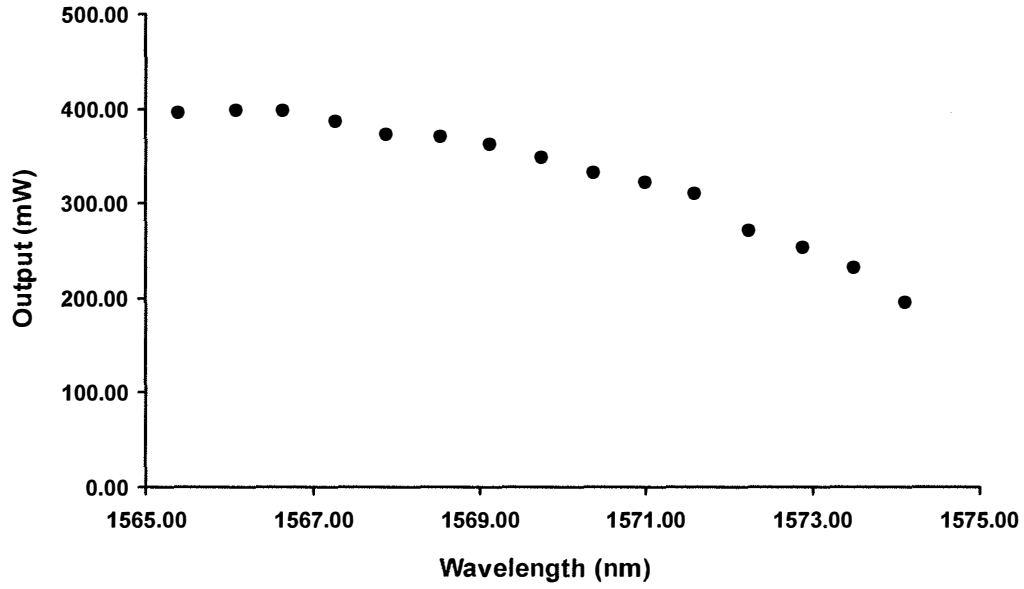
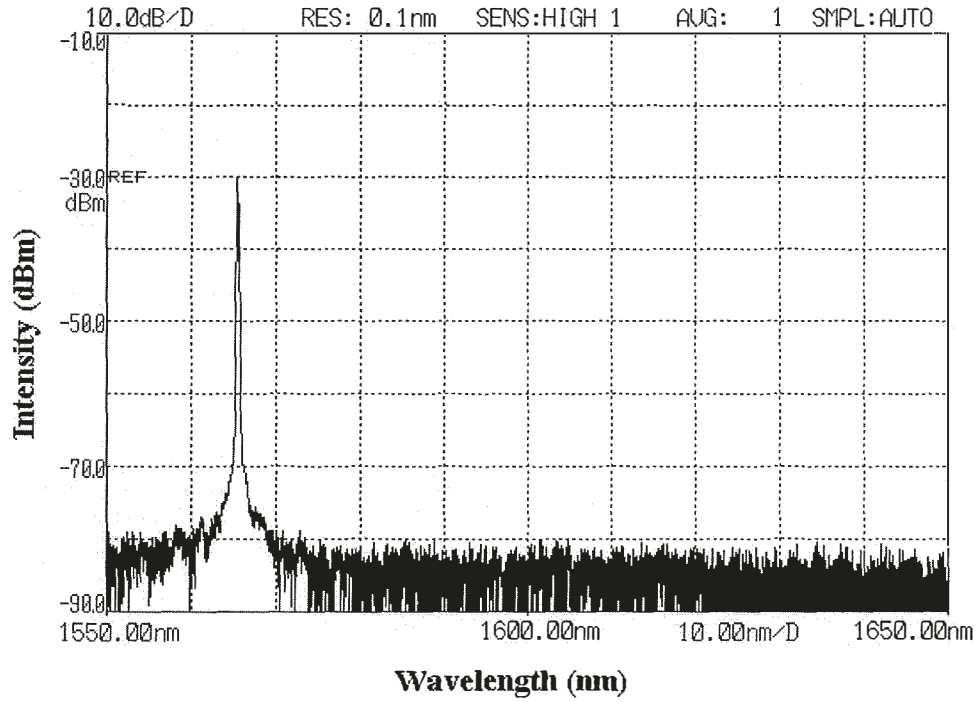
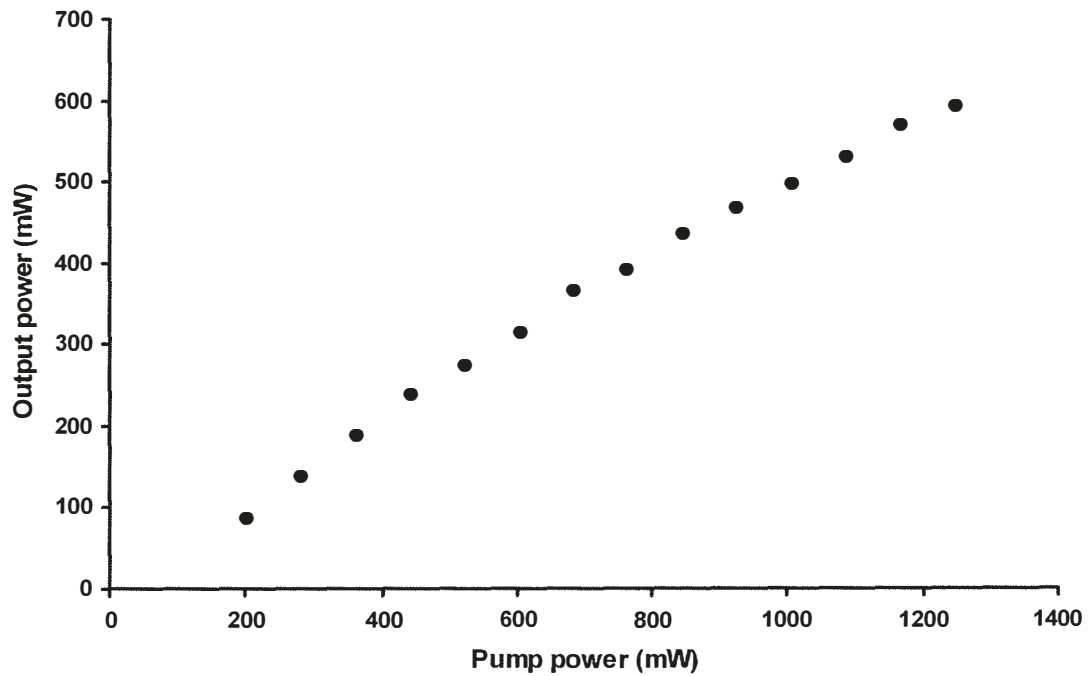


Figure 2.16: Output power of the laser at ~ 0.6 nm intervals from 1565 nm – 1575 nm.

Figure 2.17 (a) shows the output of the laser obtained by an optical spectrum analyzer (OSA) without any saturable absorber inside the cavity. Figure 2.17 (b) is the output of the laser at different pump powers coupled to the active fiber. The maximum power obtained from the laser was ~ 600 mW for a pump power of ~ 1300 mW at $\lambda = 1565.52$ nm. The threshold input power and efficiency of the laser was ~ 200 mW, and $\sim 49\%$, respectively. The effective length of our ring cavity and the length of the FP filter were ~ 9 m and ~ 0.4 m, respectively. The corresponding FSR of the cavity and FP filter was ~ 24 MHz (Equation 2.7), and ~ 514 MHz (Equation 2.6), respectively. The theoretical resonance linewidth (FWHM) of the FP filter was 2 MHz. As described earlier the output of the laser was modulated by the FP filter inside the cavity. This resulted in an effective longitudinal-mode spacing of 514 MHz for the laser cavity.



(a)



(b)

Figure 2.17: (a) Output of the laser obtained with OSA; (b) Input-Output characteristics of the laser without the SA for $\lambda = 1565.52 \text{ nm}$.

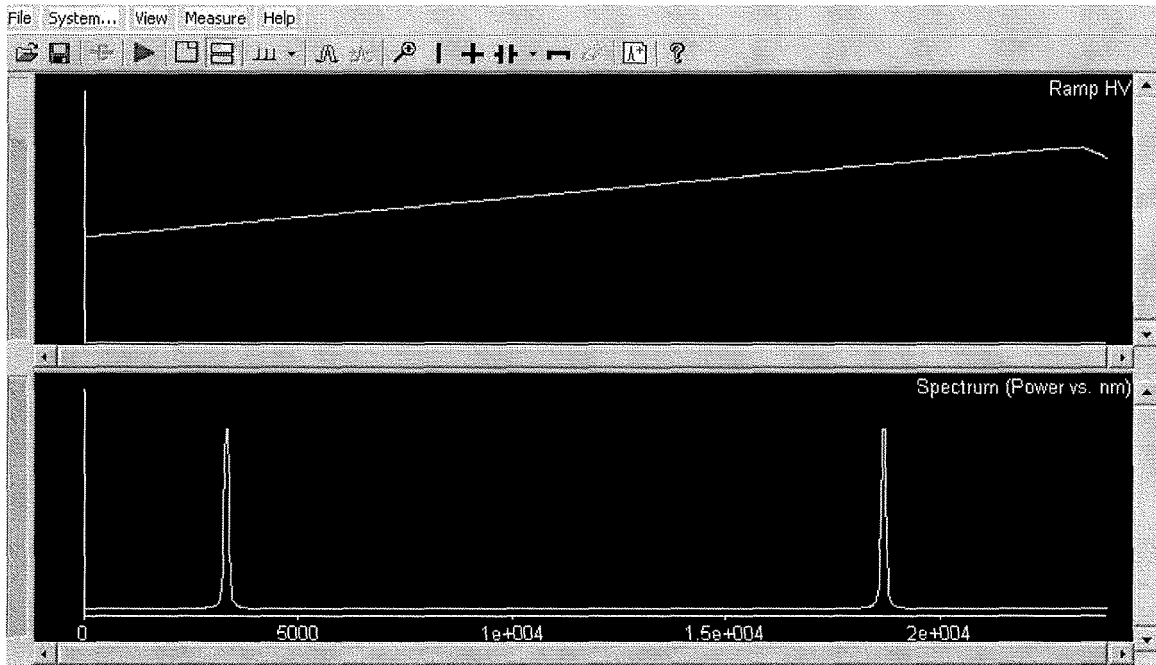


Figure 2.18: Output of the laser obtained using scanning Fabry-Perot spectrum analyzer.

To study the longitudinal-mode structure of the laser a scanning Fabry-Perot spectrum analyzer (FSR = 2 GHz) of resolution 6.7 MHz and Nuview software developed by EXFO was used. The maximum output power with single-longitudinal-mode oscillation was less than 50 mW with a 4m length of DC-EYDF. The experiment was repeated using 1m of DC-EYDF fiber to reduce the effective cavity length to 6m, which corresponds to longitudinal-mode spacing of 34 MHz. It was found that the lasing wavelength was single-longitudinal-mode and free from mode hopping to a maximum output power of 100 mW for this configuration. Figure 2.18 was obtained from the scanning Fabry-Perot spectrum analyzer (SFPSA) where the 2 GHz apart (FSR) narrow peaks in the figure correspond to the laser line and confirmed the single-longitudinal-mode oscillation of the laser. At high output power the laser output suffered from mode hopping and oscillations of multiple longitudinal modes.

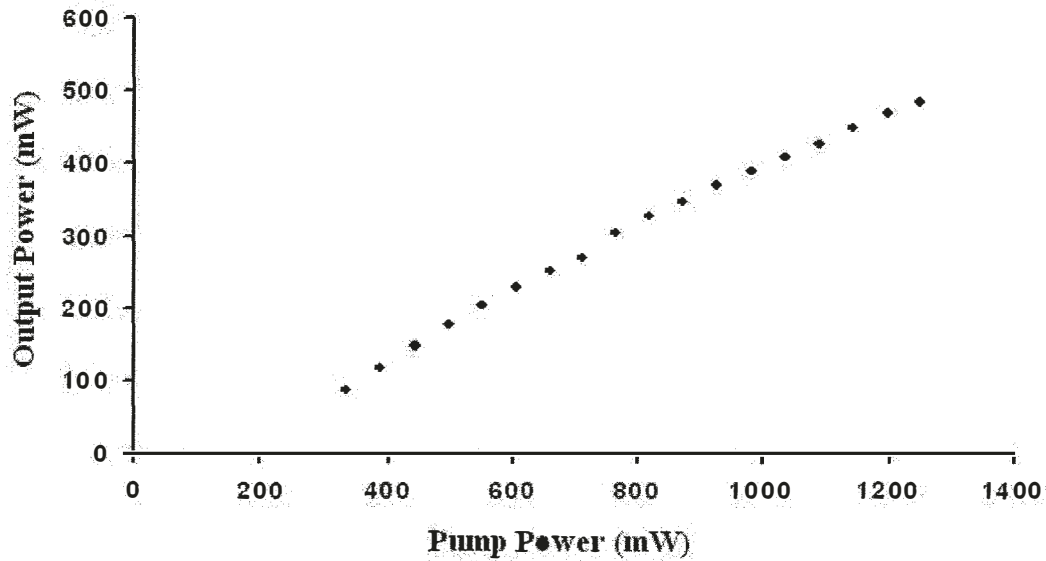


Figure 2.19: Output of the laser obtained using a power meter at $\lambda = 1565.52 \text{ nm}$.

An un-pumped rare earth doped fiber, as a saturable absorber, is a good candidate for reducing mode hopping and laser linewidth (Section 2.2.3). In our experiment an elliptical core erbium-doped fiber (PM-EDF) was used as a saturable absorber. The polarization controller and polarization-maintaining EDF helped to produce and maintain quasi-linearly polarized light inside the saturable absorber and thus increased the stability of the transient grating. In general the presence of the SA inside the cavity reduces the output power of the laser. A series of experiments were carried out using 1m, 3m, and 5m of PM-EDF to find the optimum length of the saturable absorber, which would increase the stability of the lasing wavelength, by reducing mode hopping, without largely attenuating the laser output power. We found that the 5m PM-EDF provided the stability needed while still allowing a high output power. The maximum output power achieved while still maintaining single longitudinal-mode operations was more than 300 mW with the SA. Figure 2.19 shows the input-output characteristics of the laser with 5 m of SA inside the cavity. The counter propagating light waves inside the saturable absorber

(Figure 2.1) formed the transient grating. It is evident from Equation 2.2 that the bandwidth of the transient grating is inversely proportional to the length of the saturable absorber. In our case the reflection bandwidth of the grating was 20 MHz. The transient grating acted as a tracking filter, where the central frequency tracked the lasing mode and thus eliminated mode hopping. The transient grating was capable of adjusting itself, within a few milliseconds, to any sudden changes in the laser cavity, such as changes in temperature or other environmental fluctuations [29]. The effective length of the cavity of the laser was $\sim 19\text{m}$, which corresponds to a longitudinal-mode spacing of $\sim 10\text{ MHz}$. Though the longer cavity length decreased the longitudinal-mode spacing of the cavity, the presence of the FP filter increased the longitudinal-mode spacing to 514 MHz.

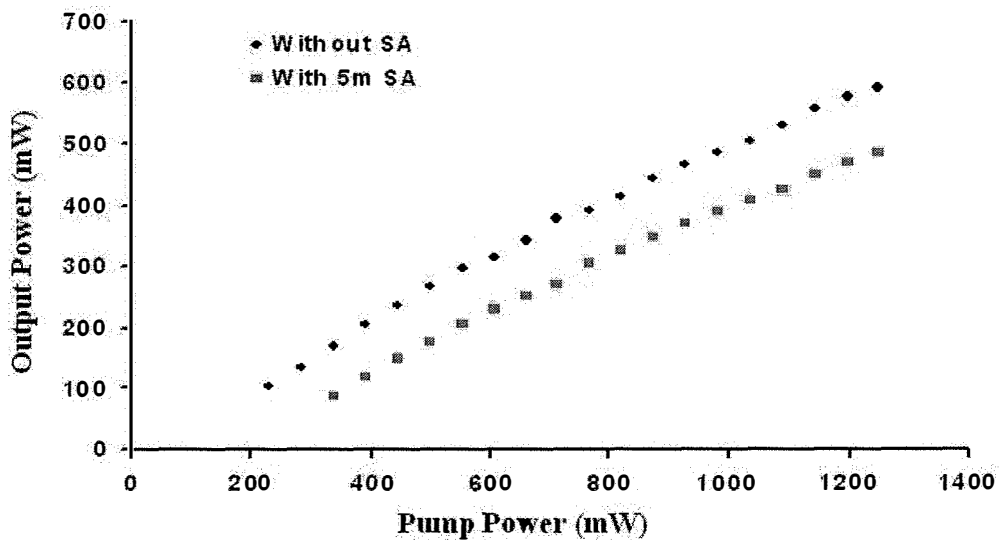


Figure 2.20: Output power of the laser with and without the saturable absorber.

Figure 2.20 shows the input-output characteristics of the laser with and without the SA. It is clear that with the saturable absorber in the cavity the output power of the laser was less. Figure 2.21 was obtained using SFPSA when the laser produced more than 300

mW of output power. It is clear from the figure that the laser was oscillating in single-longitudinal-mode.

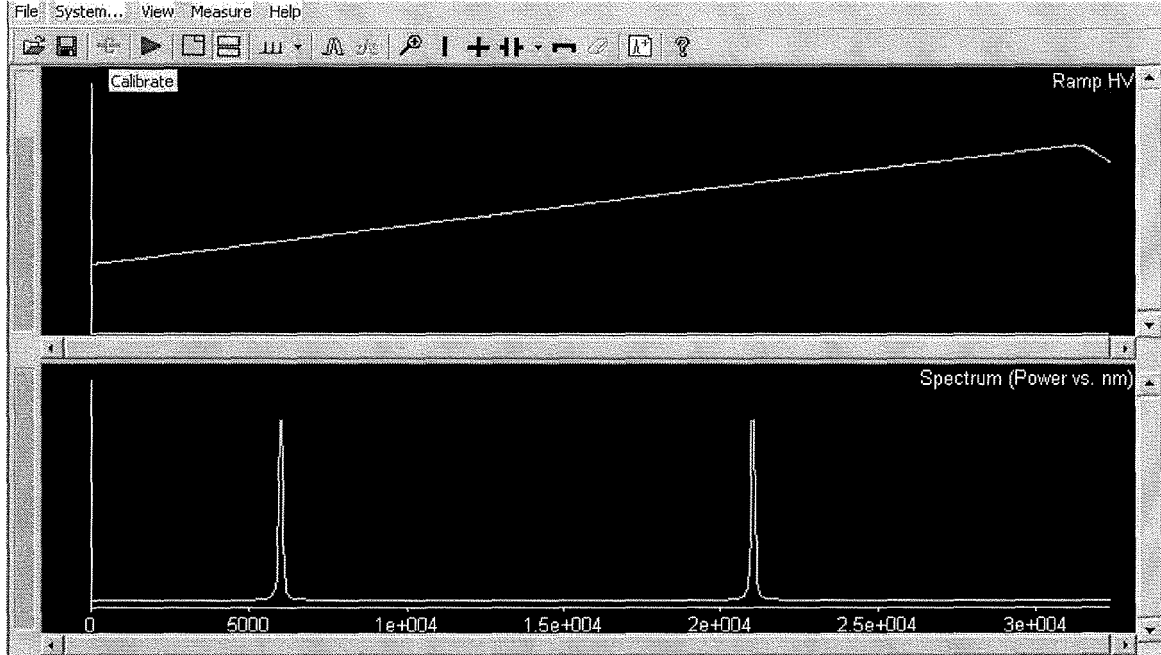


Figure 2.21: Output of the laser with the SA inside the cavity.

The 3 dB linewidth of the laser at lower power (~ 100 mW) was ~ 8.75 MHz as measured by the SFPSA and Nuviv software. The linewidth of the laser at high pump power was larger when compared to the theoretical value based on the Schawlow-Townes formula [39]. We found that the linewidth of the laser increased with increasing pump power. It was reported that the wider linewidth in the erbium-ytterbium co-doped fiber laser is due to the temperature fluctuations induced by the pump intensity noise inside the core of the fiber or due to four-wave mixing between various longitudinal modes in the laser cavities [40-43].

It was possible to maintain the relative phases of the modes by adjusting the polarization controller plates inside the cavity when the laser was oscillating in multi-longitudinal-modes. This is called passive mode-locking, and produced periodic pulses at the output of the laser. Figure 2.22 shows the output of the laser at high power obtained from the scanning Fabry-Perot spectrum analyzer, after achieving mode-locking through adjustments of the polarization controller plates inside the cavity. At the optimum location of the polarization controller plates all the modes collapsed into a single pulse with large bandwidth (~ 60 MHz). This result is due to the presence of the saturable absorber inside the cavity and is known as passive mode locking by saturable absorber or saturable absorption mode-locking. We also found that even without the presence of the saturable absorber the laser produces pulses at high powers when the polarization controller plates were adjusted properly. This is another type of passive mode locking known as nonlinear polarization rotation mode locking.

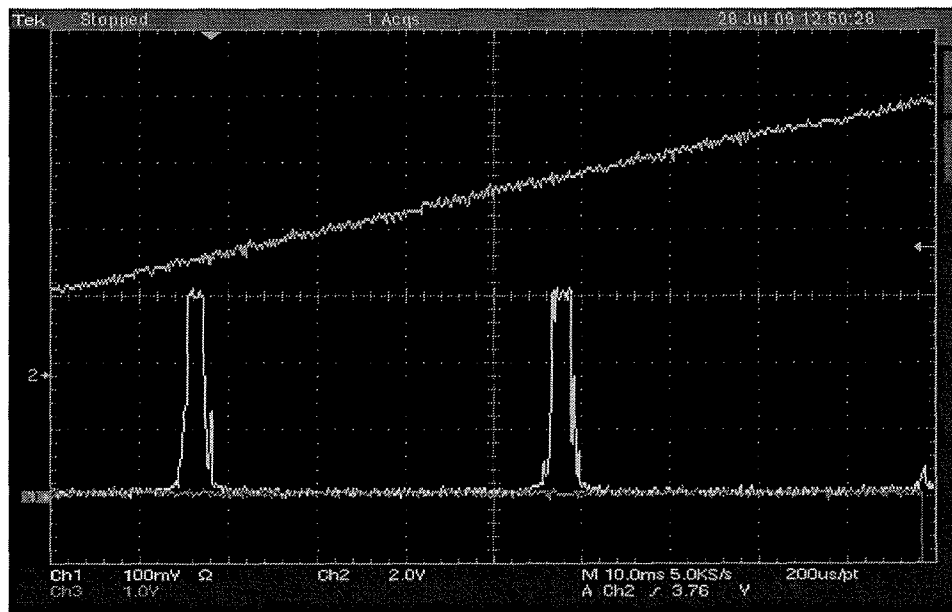


Figure 2.22: Output of the laser when the laser operated in the pulsed regime.

Figure 2.23 is the output of the laser, obtained with a high speed photo detector (2.5 GHz) and an oscilloscope of 1 GHz bandwidth when the laser was operated at high power. Thus, we could operate the laser in either CW or PULSED mode by adjusting the polarization controller plates inside the cavity. We will not discuss the mode locking mechanism and output of the laser further as it is beyond the scope of the thesis.

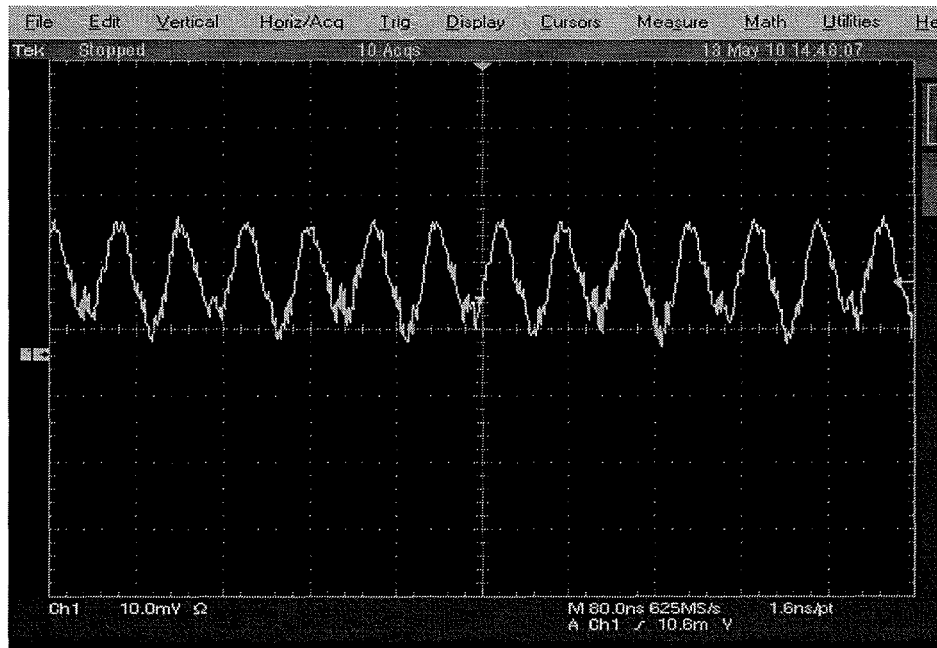


Figure 2.23: Output of the laser obtained from the oscilloscope.

Further investigation of the above laser showed that the laser can be operated in the multiwavelength regime if we replace the tunable Bragg grating (TFBG) by a broad band reflector. Figure 2.24 shows output of the laser with a broad band reflector. The laser could produce a maximum of 4 lasing wavelengths. A.J. Poustie et al. reported that a section of multimode fiber in a ring cavity can act as a filter, and it is referred to as a spatial mode beating filter [44]. In our laser cavity there were two segments of multimode fibers: (i) the multimode fiber in the fused fiber coupler with V parameter ~ 7.25 ; and (ii)

the DC-EYDF inside the resonator with V parameter ~ 4.0 ($V = 2\pi a NA/\lambda$, where a and NA are the radius and numerical aperture of the fiber and λ is the signal wavelength). Since both fibers supported the propagation of multiple modes through the fibers, interference between these modes produced the spatial mode-beating filter. The separation between two interference maximums or the FSR of the mode-beating filter was dependent on the length of the multimode fiber. Figure 2.25 (a) and Figure 2.25 (b) were obtained from the laser at different settings of the polarization controller plates, showing operation of the laser in either the single wavelength or multiwavelength regimes.

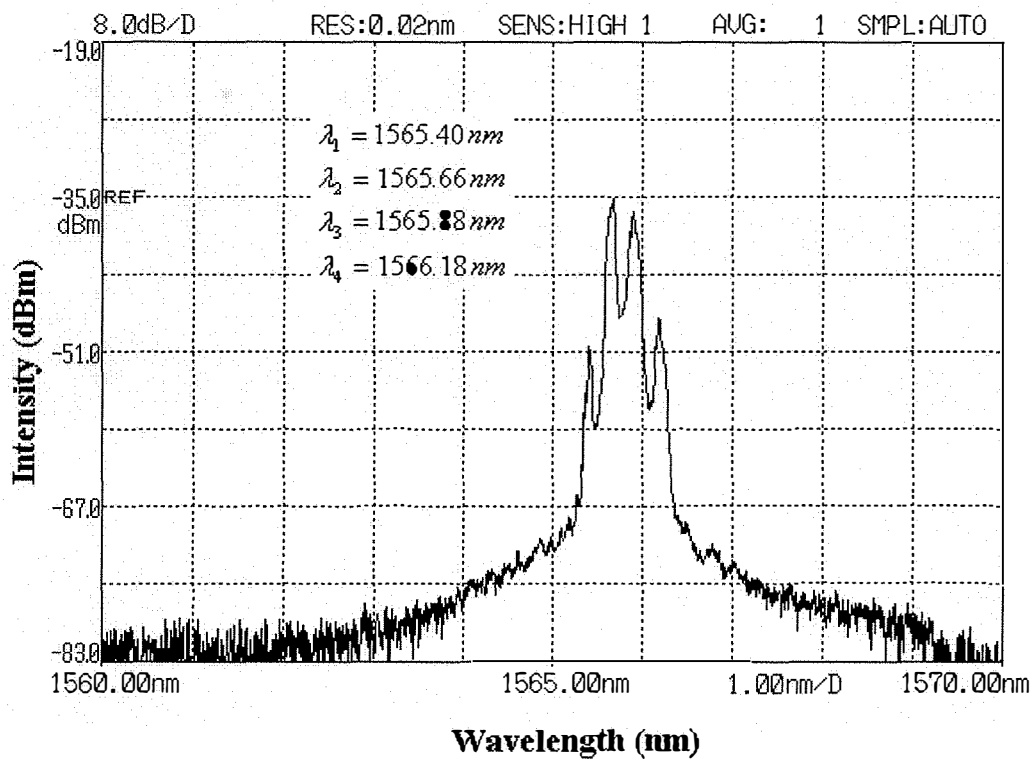
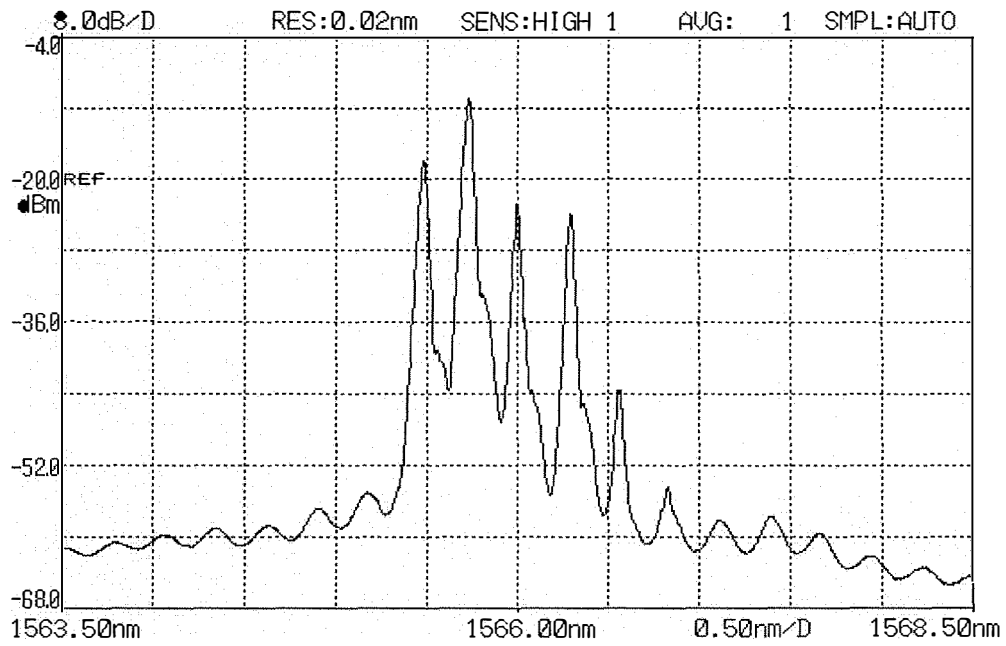


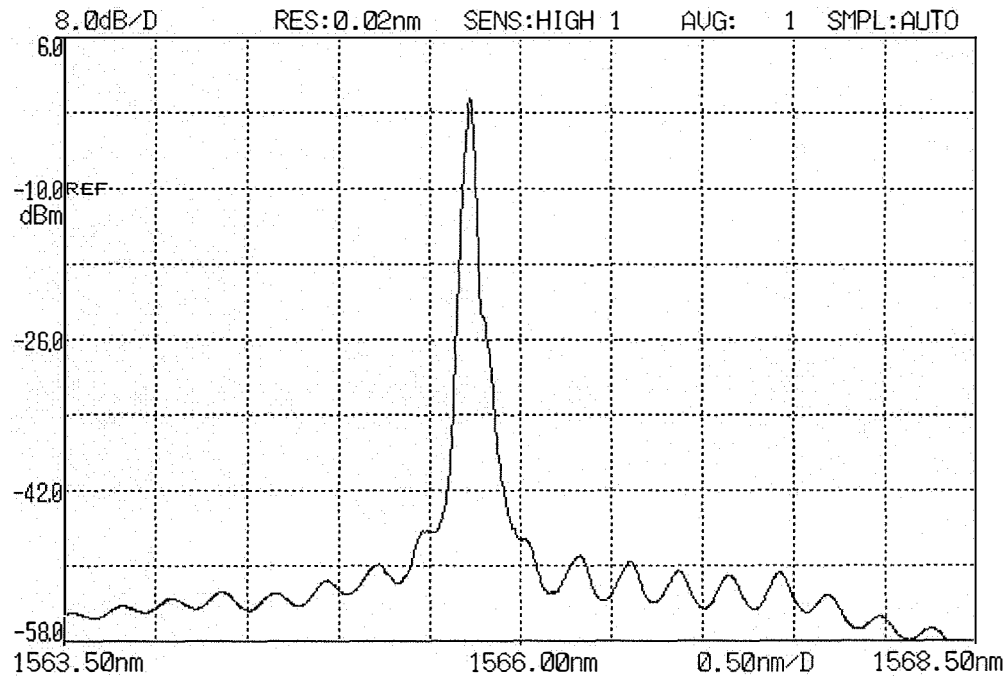
Figure 2.24: Output of the laser without the tunable fiber Bragg grating (TFBG).

It was also found that the laser can produce two wavelengths with the tunable fiber Bragg grating (TFBG) inside the cavity as shown in Figure 2.26, where one line could be

eliminated by adjusting the polarization controller plates. This could be due to the birefringence of the TFBG.



(a)



(b)

Figure 2.25: Output of the laser at different setting of the polarization controller (a) Multiwavelength laser with wavelength separation of 0.22 nm; (b) Single wavelength laser

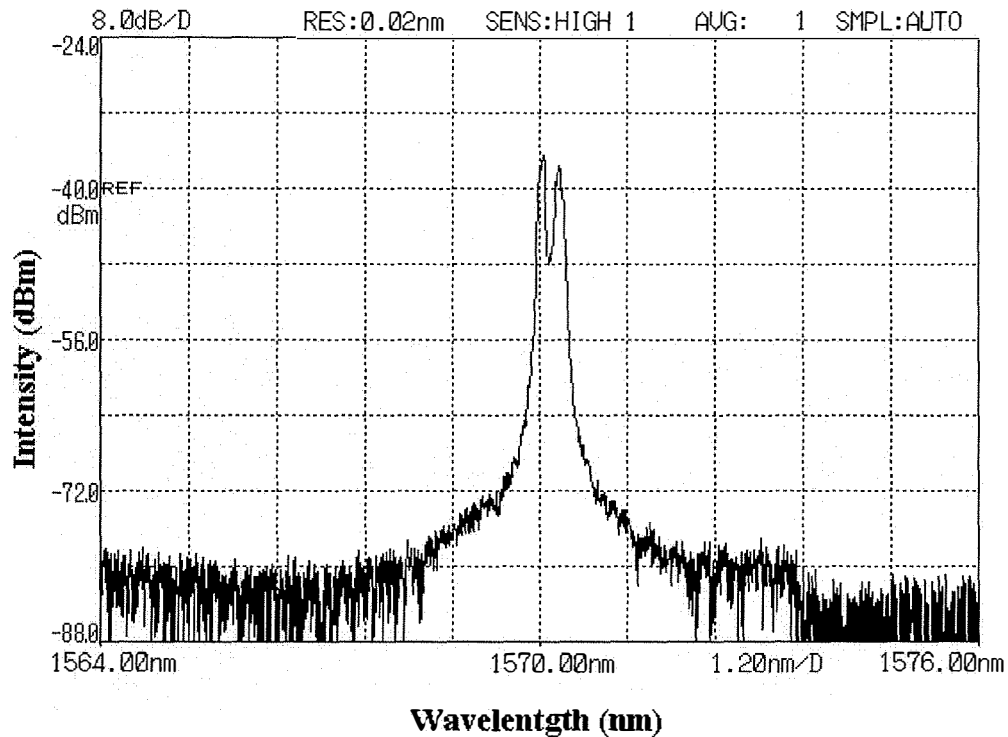


Figure 2.26: Output of the laser with tunable fiber Bragg grating (TFBG).

2.4 Discussion and Summary

We have demonstrated a high-power single-wavelength, single-longitudinal-mode fiber laser. Single-longitudinal-mode operation was achieved by using an all fiber Fabry-Perot filter inside the cavity where the laser output was modulated by the output of the filter. To reduce mode hopping an un-pumped polarization-maintaining erbium-doped fiber was used as a saturable absorber inside the cavity. The saturable absorber inside the cavity increased the stability of the laser. The laser output wavelength was single-longitudinal-mode and free from mode hopping to a maximum output power of ~ 300 mW. The laser was tunable over 10 nm range which was limited by the fiber Bragg grating. The linewidth of the laser, measured by a SFPSA was ~ 9 MHz. The effect of the length of SA inside the cavity was discussed. The ability of the laser to be operated in the

CW or PULSED mode was also discussed. Due to the narrow linewidth and high output power, this laser will be a good candidate for developing devices based on nonlinear effects in highly nonlinear optical fiber. In the following chapters we present the application of this high power laser as a pump for a Brillouin laser.

References

- [1] J. Nilsson, J. K. Sahu, Y. Jeong, W. A. Clarkson, R. Selvas, A. B. Grudinin, and S.-U. Alam, "High power fiber lasers: New Developments," *Proceedings of SPIE: Advances in Fiber Devices*, vol. 4974, pp. 50-59, 2003.
- [2] J. K. Sahu, Y. Jeong, C. Codemard, J. Nilsson, M. R. Mokhtar, M. Ibsen, D. J. Richardson, and D. N. Payne, "Tunable narrow linewidth high power erbium:ytterbium co-doped fiber laser," *Lasers and Electro-Optics/CLEO*, vol. 1 2004.
- [3] M. Laroche, P. Jander, W. A. Clarkson, J. K. Sahu, J. Nilsson, and Y. Jeong, "High power cladding-pumped tunable Er, Yb-doped fibre laser," *Electronics Letters*, vol. 40, no. 14, pp. 855-856, 2004.
- [4] Y. Jeong, J. K. Sahu, D. N. Payne, and J. Nilsson, "Ytterbium-doped large-core fiber laser with 1.36 kW continuous-wave output power," *Optics Express*, vol. 12, no. 25, pp. 6088-6092, Dec.2004.
- [5] Y. Jeong, J. Nilsson, J. K. Sahu, D. B. S. Soh, P. Dupriez, C. A. Codemard, S. Baek, D. N. Payne, R. Horley, J. A. varez-Chavez, and P. W. Turner, "Single-mode plane-polarized ytterbium-doped large-core fiber laser with 633-W continuous-wave output power," *Optics Letters*, vol. 30, no. 9, pp. 955-957, May2005.
- [6] Q. Wang, L. Zhang, C. S. Sun, and Q. X. Yu, "Multiplexed Fiber-Optic Pressure and Temperature Sensor System for Down-Hole Measurement," *IEEE Sensors Journal*, vol. 8, no. 11-12, pp. 1879-1883, Nov.2008.
- [7] S. Watson, M. J. Gander, W. N. MacPherson, J. S. Barton, J. D. C. Jones, T. Klotzbuecher, T. Braune, J. Ott, and F. Schmitz, "Laser-machined fibers as Fabry-Perot pressure sensors," *Applied Optics*, vol. 45, no. 22, pp. 5590-5596, Aug.2006.
- [8] S. Trpkovski, S. A. Wade, S. F. Collins, and G. W. Baxter, "Er³⁺: Yb³⁺ doped fibre with embedded FBG for simultaneous measurement of temperature and longitudinal strain," *Measurement Science & Technology*, vol. 16, no. 2, pp. 488-496, Feb.2005.
- [9] J. Mandal, S. Pal, T. Sun, K. T. V. Grattan, A. T. Augousti, and S. A. Wade, "Bragg grating-based fiber-optic laser probe for temperature sensing," *Ieee Photonics Technology Letters*, vol. 16, no. 1, pp. 218-220, Jan.2004.
- [10] P. M. Talaia, A. Ramos, I. Abe, M. W. Schiller, P. Lopes, R. N. Nogueira, J. L. Pinto, R. Claramunt, and J. A. Simoes, "Plated and intact femur strains in fracture fixation using fiber Bragg gratings and strain gauges," *Experimental Mechanics*, vol. 47, no. 3, pp. 355-363, June2007.
- [11] E. J. Seibel, R. E. Carroll, J. A. Dominitz, R. S. Johnston, C. D. Melville, C. M. Lee, S. M. Seitz, and M. B. Kimmey, "Tethered capsule endoscopy, a low-cost and high-performance alternative technology for the screening of esophageal cancer and Barrett's esophagus," *Ieee Transactions on Biomedical Engineering*, vol. 55, no. 3, pp. 1032-1042, Mar.2008.
- [12] Y. Sasaki, S. Tanosaki, J. Suzuki, T. Yuasa, H. Taniguchi, B. Devaraj, and T. Akatsuka, "Fundamental imaging properties of transillumination laser CT using

- optical fiber applicable to bio-medical sensing," *Ieee Sensors Journal*, vol. 3, no. 5, pp. 658-667, Oct.2003.
- [13] H. H. Kee, G. P. Lees, and T. P. Newson, "All-fiber system for simultaneous interrogation of distributed strain and temperature sensing by spontaneous Brillouin scattering," *Optics Letters*, vol. 25, no. 10, pp. 695-697, May2000.
- [14] M. Nikles, L. Thevenaz, and P. A. Robert, "Simple distributed fiber sensor based on Brillouin gain spectrum analysis," *Optics Letters*, vol. 21, no. 10, pp. 758-760, May1996.
- [15] L. Quintino, A. Costa, R. Miranda, D. Yapp, V. Kumar, and C. J. Kong, "Welding with high power fiber lasers - A preliminary study," *Materials & Design*, vol. 28, no. 4, pp. 1231-1237, 2007.
- [16] A. Polynkin, P. Polynkin, M. Mansuripur, and N. Peyghambarian, "Single-frequency fiber ring laser with 1W output power at 1.5 μm ," *Optics Express*, vol. 13, no. 8, pp. 3179-3184, Apr.2005.
- [17] Y. Jeong, C. Alegria, J. K. Sahu, L. Fu, M. Ibsen, C. Codemard, M. R. Mokhtar, and J. Nilsson, "A 43-W C-band tunable narrow-linewidth erbium-ytterbium codoped large-core fiber laser," *Ieee Photonics Technology Letters*, vol. 16, no. 3, pp. 756-758, Mar.2004.
- [18] Z. G. Lu, F. G. Sun, G. Z. Xiao, P. Lin, and P. Zhao, "High-power multiwavelength Er³⁺-Yb³⁺ codoped double-cladding fiber ring laser," *Ieee Photonics Technology Letters*, vol. 17, no. 9, pp. 1821-1823, Sept.2005.
- [19] X. X. Yang, L. Zhan, Q. S. Shen, and Y. X. Xia, "High-power single-longitudinal-mode fiber laser with a ring Fabry-Perot resonator and a saturable absorber," *Ieee Photonics Technology Letters*, vol. 20, no. 9-12, pp. 879-881, May2008.
- [20] Peter W. Milonni and Joseph H. Eberly, *Laser Physics* Wiley, 2010.
- [21] H. L. An, E. Y. B. Pun, H. D. Liu, and X. Z. Lin, "Effects of ion clusters on the performance of a heavily doped erbium-doped fiber laser," *Optics Letters*, vol. 23, no. 15, pp. 1197-1199, Aug.1998.
- [22] E. Maurice, G. Monnom, B. Dussardier, and D. B. Ostrowsky, "Clustering-induced nonsaturable absorption phenomenon in heavily erbium-doped silica fibers," *Optics Letters*, vol. 20, no. 24, pp. 2487-2489, Dec.1995.
- [23] D. Kouznetsov and J. V. Moloney, "Efficiency of pump absorption in double-clad fiber amplifiers. II. Broken circular symmetry," *Journal of the Optical Society of America B-Optical Physics*, vol. 19, no. 6, pp. 1259-1263, June2002.
- [24] J. E. Townsend, W. L. Barnes, K. P. Jdrzejewski, and S. G. Grubb, "Yb³⁺ sensitised Er³⁺ doped silica optical fibre with ultrahigh transfer efficiency and gain," *Electronics Letters*, vol. 27, no. 21, pp. 1958-1959, 1991.
- [25] K. O. Hill and G. Meltz, "Fiber Bragg grating technology fundamentals and overview," *Journal of Lightwave Technology*, vol. 15, no. 8, pp. 1263-1276, Aug.1997.
- [26] M. R. Mokhtar, C. S. Goh, S. A. Butler, S. Y. Set, K. Kikuchi, D. J. Richardson, and M. Ibsen, "Fibre Bragg grating compression-tuned over 110 nm," *Electronics Letters*, vol. 39, no. 6, pp. 509-511, Mar.2003.

- [27] L. G. Luo and P. L. Chu, "Passive Q-switched erbium-doped fibre laser with saturable absorber," *Optics Communications*, vol. 161, no. 4-6, pp. 257-263, Mar.1999.
- [28] S. J. Frisken, "Transient Bragg Reflection Gratings in Erbium-Doped Fiber Amplifiers," *Optics Letters*, vol. 17, no. 24, pp. 1776-1778, Dec.1992.
- [29] Y. Cheng, J. T. Kringlebotn, W. H. Loh, R. I. Laming, and D. N. Payne, "Stable Single-Frequency Traveling-Wave Fiber Loop Laser with Integral Saturable-Absorber-Based Tracking Narrow-Band-Filter," *Optics Letters*, vol. 20, no. 8, pp. 875-877, Apr.1995.
- [30] X. Y. Fan, Z. Y. He, Y. Mizuno, and K. Hotate, "Bandwidth-adjustable dynamic grating in erbium-doped fiber by synthesis of optical coherence function," *Optics Express*, vol. 13, no. 15, pp. 5756-5761, July2005.
- [31] B. Fischer, J. L. Zuskind, and D. J. Digiovanni, "Nonlinear 4-Wave-Mixing in Erbium-Doped Fiber Amplifiers," *Electronics Letters*, vol. 29, no. 21, pp. 1858-1859, Oct.1993.
- [32] H. C. Lefevre, "Single-Mode Fiber Fractional Wave Devices and Polarization Controllers," *Electronics Letters*, vol. 16, no. 20, pp. 778-780, 1980.
- [33] G. Keiser, *Optical Fiber Communications*, 3 ed. Boston, MA: McGraw Hill, 2000.
- [34] G. Das and Z. J. Chaboyer, "Single-wavelength fiber laser with 250 mW output power at 1.57 μm ," *Optics Express*, vol. 17, no. 10, pp. 7750-7755, 2009.
- [35] L. F. Stokes, M. Chodorow, and H. J. Shaw, "All-Single-Mode Fiber Resonator," *Optics Letters*, vol. 7, no. 6, pp. 288-290, 1982.
- [36] P. Urquhart, "Compound Optical-Fiber-Based Resonators," *Journal of the Optical Society of America A-Optics Image Science and Vision*, vol. 5, no. 6, pp. 803-812, June1988.
- [37] S. J. Hogeveen and H. Vandestadt, "Fabry-Perot Interferometers with 3 Mirrors," *Applied Optics*, vol. 25, no. 22, pp. 4181-4184, Nov.1986.
- [38] H. Vandestadt and J. M. Muller, "Multimirror Fabry-Perot Interferometers," *Journal of the Optical Society of America A-Optics Image Science and Vision*, vol. 2, no. 8, pp. 1363-1370, 1985.
- [39] A. L. Schawlow and C. H. Townes, "Infrared and Optical Masers," 112 ed 1958, pp. 1940-1949.
- [40] N. Y. Voo, P. Horak, M. Ibsen, and W. H. Loh, "Anomalous linewidth behavior in short-cavity single-frequency fiber lasers," *Ieee Photonics Technology Letters*, vol. 17, no. 3, pp. 546-548, Mar.2005.
- [41] P. Horak, N. Y. Voo, M. Ibsen, and W. H. Loh, "Pump-noise-induced linewidth contributions in distributed feedback fiber lasers," *Ieee Photonics Technology Letters*, vol. 18, no. 9-12, pp. 998-1000, May2006.
- [42] M. A. LaPointe and M. Piche, "Linewidth of high-power fiber lasers," *Proceedings of SPIE: Photonics North 2009*, vol. 7386, pp. 73860S-1-73860S-8, 2009.
- [43] V. Roy, M. Piche, F. Babin, and G. W. Schinn, "Nonlinear wave mixing in a multilongitudinal-mode erbium-doped fiber laser," *Optics Express*, vol. 13, no. 18, pp. 6791-6797, Sept.2005.

- [44] A. J. Poustie, N. Finlayson, and P. Harper, "Multiwavelength Fiber Laser Using A Spatial Mode Beating Filter," *Optics Letters*, vol. 19, no. 10, pp. 716-718, May1994.

Chapter 3

Brillouin fiber laser made with Highly Nonlinear Photonic Crystal Fiber

3.1 Introduction

A Photonic Crystal Fiber (PCF) is a silica glass fiber with a periodic array of holes in the axial direction that allows one to manipulate propagation of light. Figure 3.1 shows the structures of two different classes of PCF. In PCF light can be guided either by modified total internal reflection or through the photonic bandgap effect. In addition, there are a number of subclasses of PCF that vary with structure and optical properties, such as highly nonlinear (HNL), large mode area (LMA), low-index cladding (LIC), and air-guiding (AG) photonic crystal fibers. This fiber has attracted much attention because of properties like wide single mode operation, high nonlinearity and tailorable dispersion. There are a number of applications that have been reported in the literature such as

supercontinuum generation, where a PCF was pumped with a pulsed laser at 647 nm [1;2], and as temperature and strain sensors [3-5].

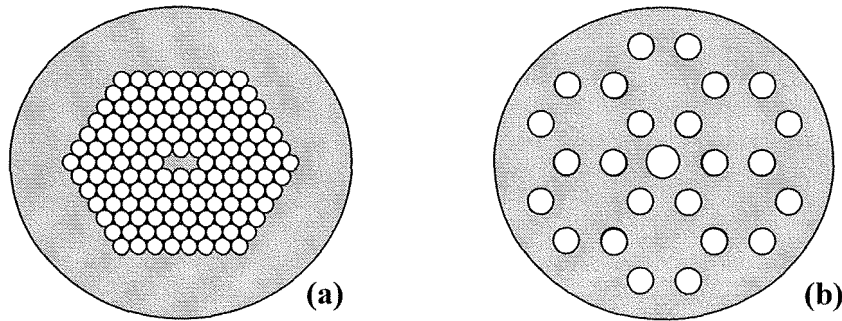


Figure 3.1: The structure of (a) a highly nonlinear solid core PCF, (b) a hollow core PCF fiber.

Stimulated Brillouin scattering (Section 1.4.1) occurs when an optical power launched into the fiber exceeds a Brillouin threshold level. In highly nonlinear PCF this threshold power level is easier to reach as the modal field is tightly confined inside the core. The SBS has a detrimental effect on devices based on highly nonlinear fiber due to the saturation effect and backscattered radiation [6]. However, for applications such as amplification, lasing, slow light generation and sensing, SBS is very useful [7-12]. In general, a longer length of single-mode fiber (SMF) is required to develop devices that use the SBS effect, due to the very low nonlinear coefficient of silica. Recently, fibers with high nonlinear coefficients have been used to develop photonic devices to overcome longer length requirements [7;13]. Nonlinear photonic crystal fibers are very attractive for developing photonic devices due to their unique optical properties. The recent investigation of SBS in highly birefringent photonic crystal fiber shows that the fiber is a good candidate for developing fiber lasers and sensors [14;15]. The fiber we chose to use for our Brillouin fiber laser is a highly nonlinear elliptical core PCF (Figure 3.1a), a polarization-maintaining fiber was chosen to reduce the Brillouin threshold power. The

fiber has a solid core and guides light by the principles of modified total internal reflection.

A multiwavelength fiber laser source is very attractive for its applications in optical communications, photonic device characterizations and sensing. Several techniques have been proposed and demonstrated to produce multiwavelength fiber lasers using erbium-doped fiber as a gain medium [16-18]. SBS is one of the techniques which have been used to produce multiwavelength fiber lasers [19-23].

In this chapter, we present a dual-wavelength Brillouin fiber laser in a unidirectional ring cavity configuration using a highly nonlinear, polarization-maintaining PCF. An in-house designed and constructed erbium/ytterbium co-doped fiber laser was used as a Brillouin pump source (Chapter 2). Further, we investigated the effects of the polarization-maintaining property of the PCF on the output of the Brillouin fiber laser.

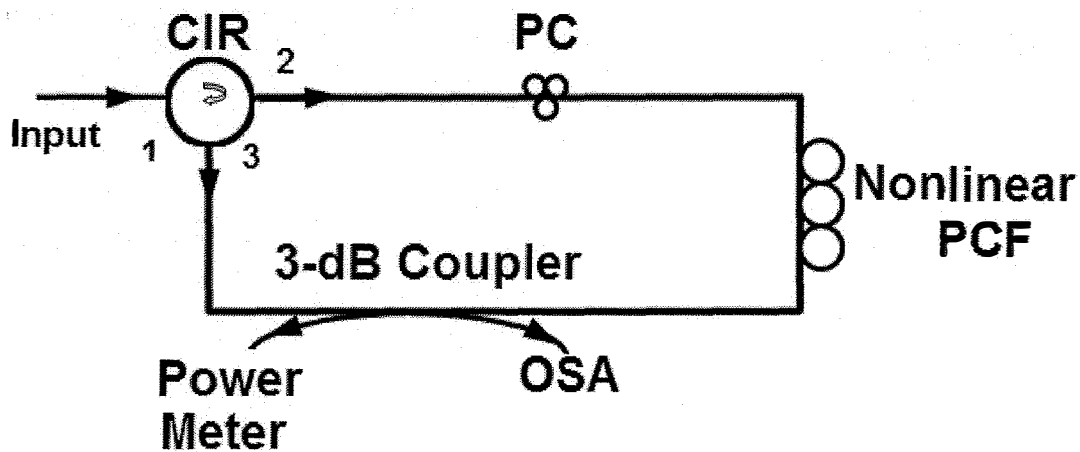


Figure 3.2: Experimental setup. CIR: Polarization insensitive optical circulator; PC: Polarization controller; OSA: Optical spectrum analyzer.

3.2 Experimental Setup

The schematic of the Brillouin fiber laser is shown in Figure 3.2. The Brillouin laser cavity was configured in a ring resonator setup and consisted of a three port polarization insensitive circulator (CIR, Figure 3.2), a three meter long nonlinear elliptical core PCF, an all-fiber polarization controller to control the polarization state of the lightwaves inside the cavity and a 3-dB coupler to extract the output of the laser. The PCF had an effective nonlinear coefficient of $0.12 \text{ m}^{-1} \text{ W}^{-1}$, core dimension of $1.3 \times 2.3 \mu\text{m}$, birefringence of 2.2×10^{-3} at 1530 nm, attenuation of 84 dB/Km at 1550 nm (which results in an effective length of 2.91 m) and beat length of 0.7mm. The high intensity light within the core modulates the core refractive index. The effective nonlinear coefficient is determined by Equation 3.1 [24],

$$\gamma = \frac{2\pi n_2}{\lambda A_{eff}} \quad (3.1)$$

where n_2 is the nonlinear index of refraction, λ is the wavelength of the incident light, and A_{eff} is the effective mode area. The typical value of effective nonlinear coefficient for Corning SMF 28 is $0.001 \text{ m}^{-1} \text{ W}^{-1}$ [24], which is two orders of magnitude less than that of our photonic crystal fiber.

The pump radiation entered the cavity from port 1 of the polarization independent optical circulator, as shown in Figure 3.2. The radiation was emitted out of port 2 of the optical circulator which was spliced to a PC. The polarization controller was then spliced to the PCF fiber, which controlled the polarization of the light entering the photonic crystal fiber. The Brillouin scattered light was reflected back through the PC, where it

entered port 2 and was directed towards port 3. The output power of the laser was extracted through a 3-dB coupler. The output power of the Brillouin laser was monitored using an Optical Spectrum Analyzer (OSA) of resolution 0.01 nm. A power meter was used to monitor forward propagating waves inside the cavity. We used a repeated arc discharge technique to splice PCF and SMF together. The multiple arc discharge (Figure 3.3) increased the mode field diameter (the controlled collapse of the air holes reduced the effective refractive index contrast between core and cladding) of the PCF at the interface so that it matches the mode field diameter of SMF, and thus reduced the splice loss [25;26].

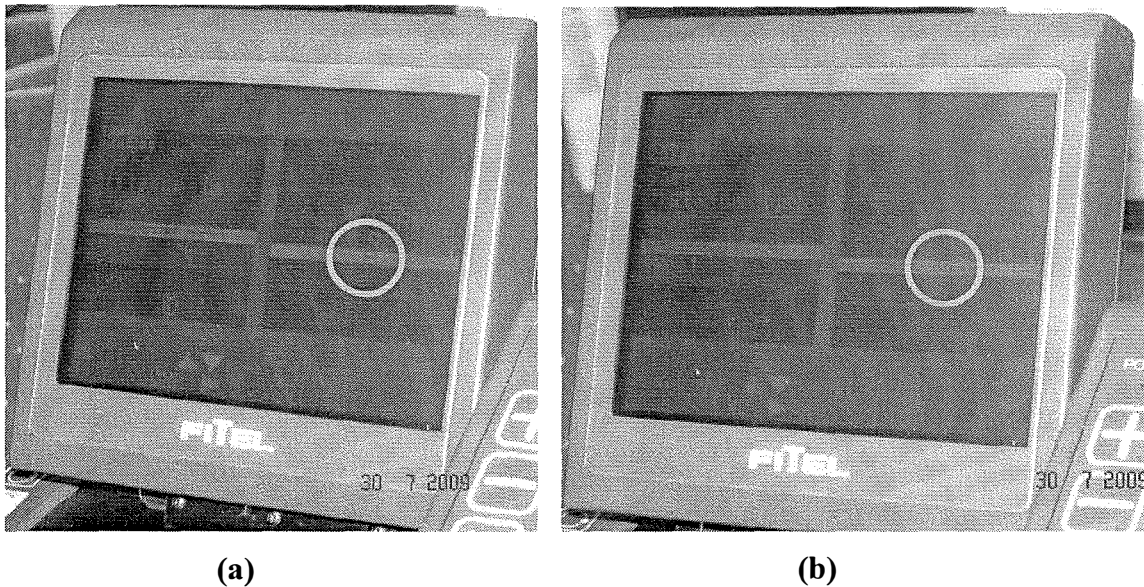


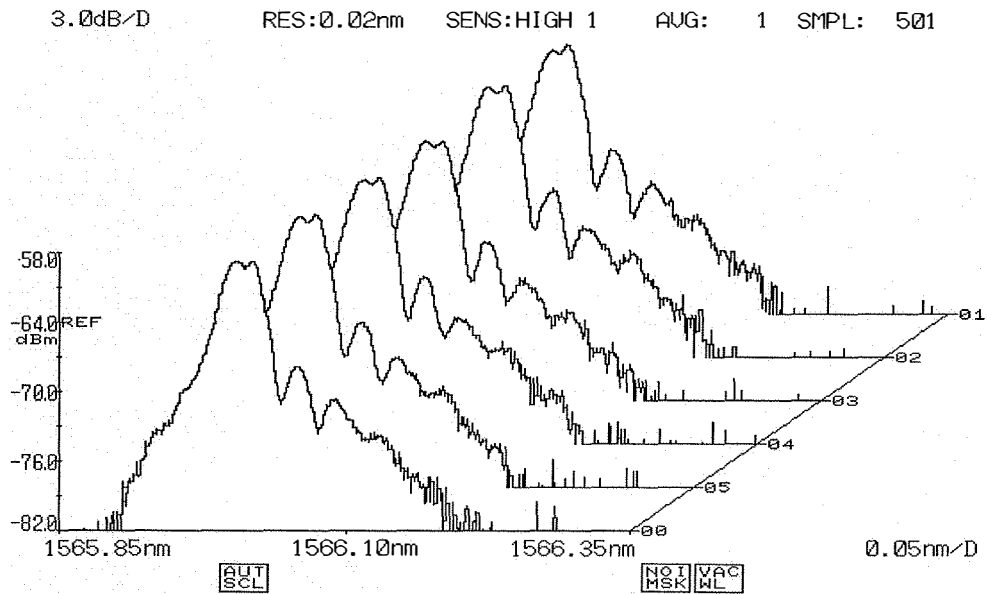
Figure 3.3: Controlled collapse of PCF air holes when splicing to SMF, (a) a hole can be seen at SMF-PCF interface, (b) multiple arcs eliminated the hole.

3.3 Results and Analysis

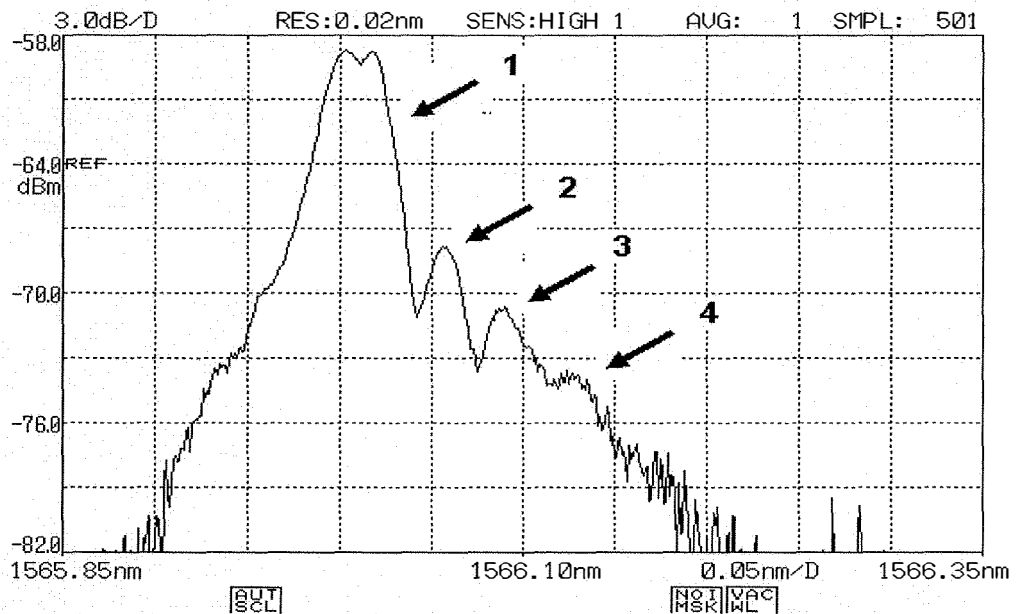
Figure 3.4 shows the output of the Brillouin laser obtained using three meters of nonlinear polarization-maintaining PCF for an input pump power of ~ 450 mW at wavelength 1565.96 nm. The output of the laser shows multiple peaks, despite the fact that the laser cavity can support only one lasing-wavelength. It was found that a small-core photonic crystal fiber produces multiple peaks in the SBS output spectrum due to the highly multimode character of the acoustic wave [14;15]. The separation between two consecutive peaks was 0.04 nm (~ 5 GHz). The intensities of the 2nd, 3rd and 4th peaks were more than 10 dB lower than the central peak. Further, it is clear from Figure 3.4 that there is splitting of the central peak and by adjusting the polarization controller plates we could produce a single peak or two peaks with equal intensities (Figure 3.5). The two frequencies in the first order were due to the birefringent property of the PCF. The x and y components of the incident waves experienced different amounts of Brillouin frequency shift due to the difference in refractive indices of core ($n_x \neq n_y$). By adjusting the polarization controller plates we favored a particular polarization-mode to be excited. The other higher order modes did not show any splitting due to their high threshold power [15].

The lasing lines were very stable with an intensity fluctuation of less than 0.2 dB. The effective cavity length of the ring resonator was ~ 7 m, which corresponds to a longitudinal mode spacing of ~ 30 MHz. The threshold pump power of the laser was very high due to the splice losses between the PCF and SMF, and consequentially, reduced the output power of the laser. The linewidth of the pump laser was ~ 14 MHz. The output of

the Brillouin laser shows a broader laser spectrum which is due to the limited resolution (1.25 GHz) of the OSA.

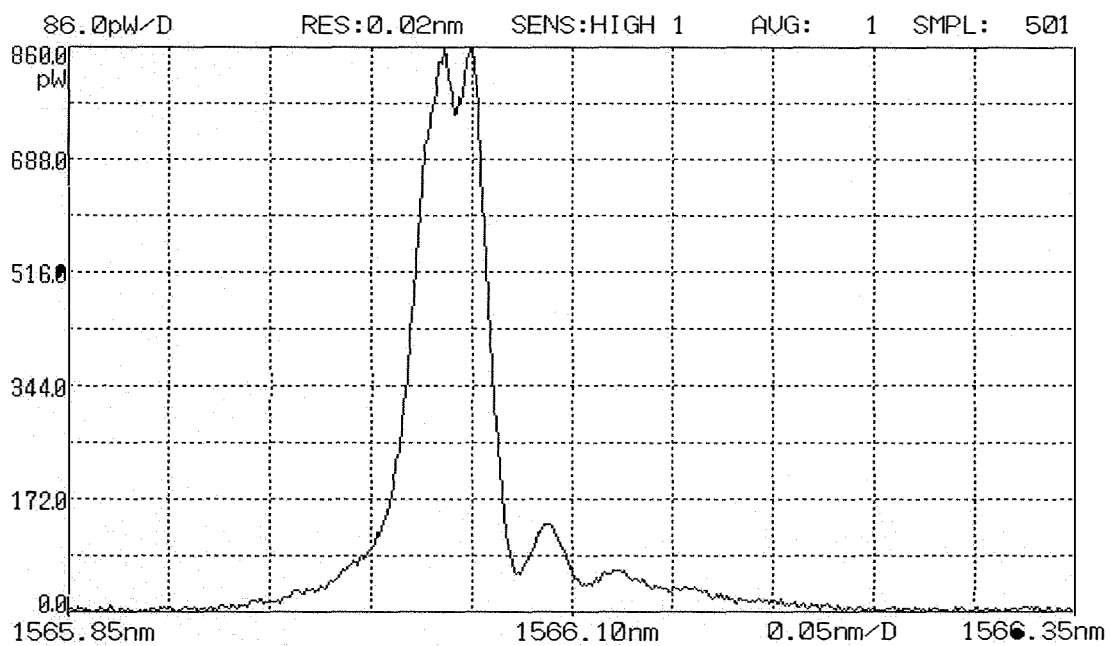


(a)

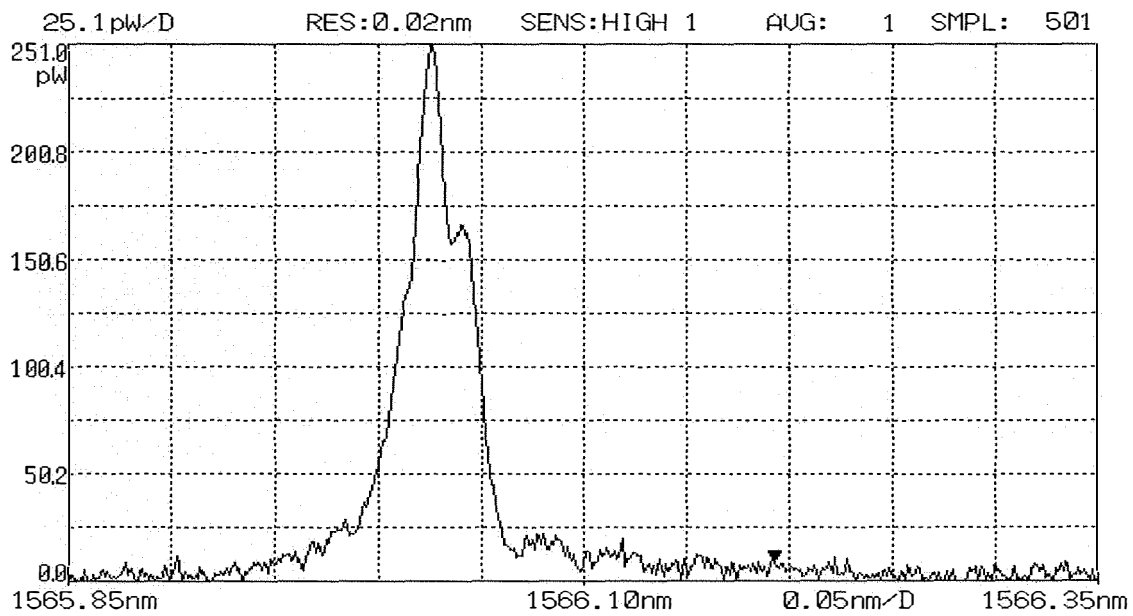


(b)

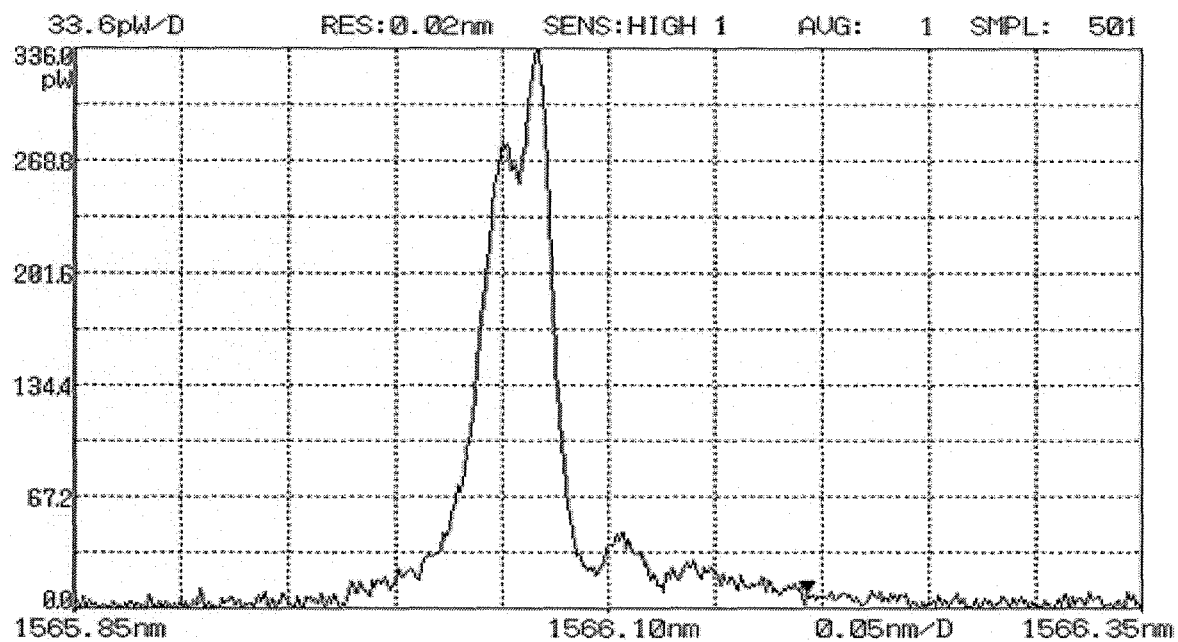
Figure 3.4: Output of the Brillouin fiber laser for an input pump power of 450 mW at 1565.96 nm wavelength, (a) Multiple scan at 2 minutes interval; (b) single scan.



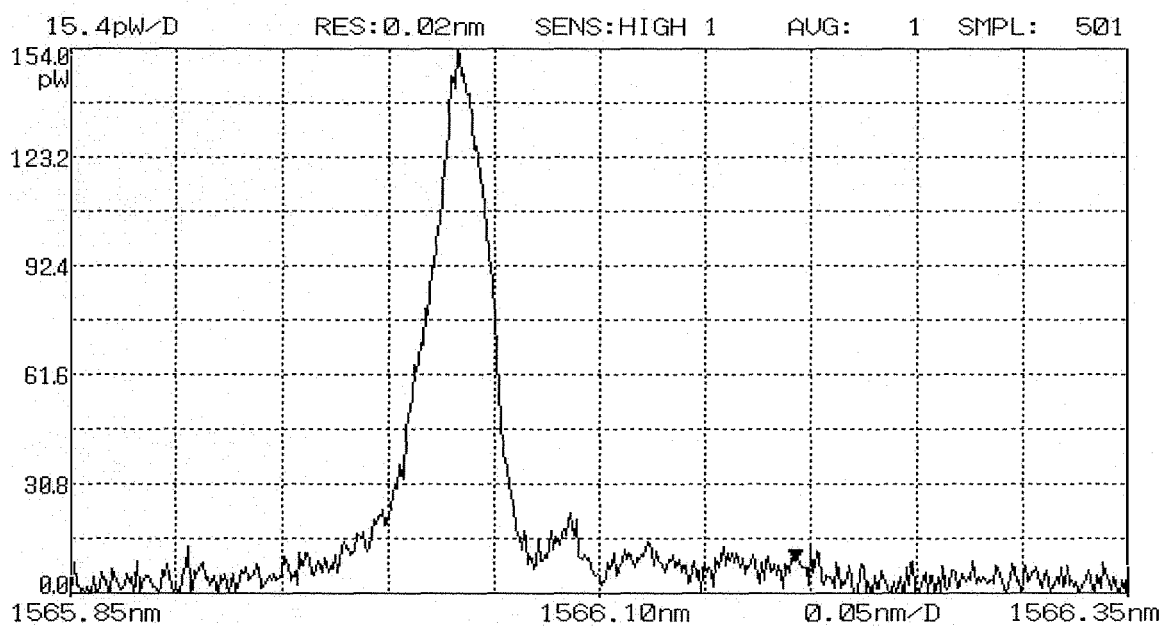
(a)



(b)



(c)



(d)

Figure 3.5: Output of the multiwavelength Brillouin fiber laser at different polarization controller plates position.

3.4 Discussion and Summary

In conclusion, we have demonstrated a Brillouin fiber laser using highly nonlinear polarization maintaining photonic crystal fiber. The laser could produce a multiwavelength output with a separation of 0.04 nm. The multiple peaks were due to the multimode property of the small core PCF used in this experiment. By adjusting the polarization controller plates we could make the laser oscillate in single-wavelength or dual-wavelength regimes, where the separation between two lasing wavelengths depended on the birefringent properties of the PCF. The high nonlinearity of the PCF fiber reduced the length of the resonant cavity and resulted in wider longitudinal mode spacing. The birefringent property of the PCF fiber increased the stability of the lasing line.

References

- [1] S. Coen, A. H. L. Chau, R. Leonhardt, J. D. Harvey, J. C. Knight, W. J. Wadsworth, and P. S. J. Russell, "Supercontinuum generation by stimulated Raman scattering and parametric four-wave mixing in photonic crystal fibers," *Journal of the Optical Society of America B-Optical Physics*, vol. 19, no. 4, pp. 753-764, Apr.2002.
- [2] J. K. Ranka, R. S. Windeler, and A. J. Stentz, "Visible continuum generation in air-silica microstructure optical fibers with anomalous dispersion at 800 nm," *Optics Letters*, vol. 25, no. 1, pp. 25-27, Jan.2000.
- [3] J. Ju, Z. Wang, W. Jin, and M. S. Demokan, "Temperature sensitivity of a two-mode photonic crystal fiber interferometric sensor," *Ieee Photonics Technology Letters*, vol. 18, no. 17-20, pp. 2168-2170, Sept.2006.
- [4] S. S. Li, Z. D. Huang, X. S. Song, S. Y. Zhang, Q. Zhong, F. Xu, and Y. Q. Lu, "Photonic crystal fibre based high temperature sensor with three-beam path interference," *Electronics Letters*, vol. 46, no. 20, pp. 1394-1396, Sept.2010.
- [5] O. Frazao, J. M. Baptista, and J. L. Santos, "Temperature-independent strain sensor based on a Hi-Bi photonic crystal fiber loop mirror," *IEEE Sensors Journal*, vol. 7, no. 9-10, pp. 1453-1455, Sept.2007.
- [6] S. Bickham, A. Kobayakov, and S. Li, "Nonlinear Optical Fibers with Increased SBS Thresholds," 2006.
- [7] K. S. Abedin, "Brillouin amplification and lasing in a single-mode AS(2)Se(3) chalcogenide fiber," *Optics Letters*, vol. 31, no. 11, pp. 1615-1617, June2006.
- [8] G. S. Qin, A. Mori, and Y. Ohishi, "Brillouin lasing in a single-mode tellurite fiber," *Optics Letters*, vol. 32, no. 15, pp. 2179-2181, Aug.2007.
- [9] P. Bayvel and I. P. Giles, "Evaluation of Performance Parameters of Single-Mode All-Fiber Brillouin Ring Lasers," *Optics Letters*, vol. 14, no. 11, pp. 581-583, June1989.
- [10] A. Yeniay, J. M. Delavaux, and J. Toulouse, "Spontaneous and stimulated Brillouin scattering gain spectra in optical fibers," *Journal of Lightwave Technology*, vol. 20, no. 8, pp. 1425-1432, Aug.2002.
- [11] K. Y. Song, W. W. Zou, Z. Y. He, and K. Hotate, "All-optical dynamic grating generation based on Brillouin scattering in polarization-maintaining fiber," *Optics Letters*, vol. 33, no. 9, pp. 926-928, May2008.
- [12] T. R. Parker, M. Farhadiroushan, V. A. Handerek, and A. J. Rogers, "Temperature and strain dependence of the power level and frequency of spontaneous Brillouin scattering in optical fibers," *Optics Letters*, vol. 22, no. 11, pp. 787-789, June1997.
- [13] G. S. Qin, H. Sotobayashi, M. Tsuchiya, A. Mori, T. Suzuki, and Y. Ohishi, "Stimulated Brillouin scattering in a single-mode tellurite fiber for amplification, lasing, and slow light generation," *Journal of Lightwave Technology*, vol. 26, no. 5-8, pp. 492-498, Mar.2008.
- [14] A. Minardo, R. Bernini, W. Urbanczyk, J. Wojcik, N. Gorbato, M. Tur, and L. Zeni, "Stimulated Brillouin scattering in highly birefringent microstructure fiber: experimental analysis," *Optics Letters*, vol. 33, no. 20, pp. 2329-2331, Oct.2008.

- [15] J. E. McElhenny, R. K. Pattnaik, J. Toulouse, K. Saitoh, and M. Koshiba, "Unique characteristic features of stimulated Brillouin scattering in small-core photonic crystal fibers," *Journal of the Optical Society of America B-Optical Physics*, vol. 25, no. 4, pp. 582-593, Apr.2008.
- [16] G. Das and J. W. Y. Lit, "L-band multiwavelength fiber laser using an elliptical fiber," *Ieee Photonics Technology Letters*, vol. 14, no. 5, pp. 606-608, May2002.
- [17] O. Graydon, W. H. Loh, R. I. Laming, and L. Dong, "Triple-frequency operation of an Er-doped twincore fiber loop laser," *Ieee Photonics Technology Letters*, vol. 8, no. 1, pp. 63-65, Jan.1996.
- [18] N. Park and P. F. Wysocki, "24-line multiwavelength operation of erbium-doped fiber-ring laser," *Ieee Photonics Technology Letters*, vol. 8, no. 11, pp. 1459-1461, Nov.1996.
- [19] Y. J. Song, L. Zhan, S. Hu, Q. H. Ye, and Y. X. Xia, "Tunable Mltiwavelength Brillouin-Erbium fiber laser with a polarization-maintaining fiber Sagnac loop filter," *IEEE Phot. Tech. Lett.*, vol. 16, no. 9, pp. 2015-2017, 2004.
- [20] N. S. Kim, "Multiwavelength operation of EDFA-enhanced Brillouin erbium fibre lasers," *Electronics Letters*, vol. 34, no. 7, pp. 673-675, Apr.1998.
- [21] M. N. M. Nasir, Z. Yusoff, M. H. Al-Mansoori, H. A. A. Rashid, and P. K. Choudhury, "Widely tunable multi-wavelength Brillouin-erbium fiber laser utilizing low SBS threshold," *Optics Express*, vol. 17, no. 15, pp. 12829-12834, July2009.
- [22] S. W. Harun, S. Shahi, and H. Ahmad, "Compact Brillouin-erbium fiber laser," *Optics Letters*, vol. 34, no. 1, pp. 46-48, Jan.2009.
- [23] G. J. Cowle, D. Y. Stepanov, and Y. T. Chieng, "Brillouin/erbium fiber lasers," *Journal of Lightwave Technology*, vol. 15, no. 7, pp. 1198-1204, July1997.
- [24] A. Bjarklev, J. Broeng, and A. S. Bjarldev, *Photonic Crystal Fibres* Kluwer Academic Publishers, 2003.
- [25] L. M. Xiao, W. Jin, and M. S. Demokan, "Fusion splicing small-core photonic crystal fibers and single-mode fibers by repeated arc discharges," *Optics Letters*, vol. 32, no. 2, pp. 115-117, Jan.2007.
- [26] L. Xiao, M. S. Demokan, W. Jin, Y. Wang, and C. L. Zhao, "Fusion splicing photonic crystal fibers and conventional single-mode fibers: Microhole collapse effect," *Journal of Lightwave Technology*, vol. 25, no. 11, pp. 3563-3574, Nov.2007.

Chapter 4

Brillouin fiber laser with an Arsenic Selenium Chalcogenide (As_2Se_3) glass fiber

4.1 Introduction

Within a few years of the development of chalcogenide glass fibers (As_2Se_3), they have become commercially available. These fibers are ideal for applications such as chemical sensing, temperature monitoring, nonlinear optical switching, and transmission of near-infrared (NIR) to far-infrared (FIR) wavelengths. Chalcogenide glass refers to a type of glass made with one or more of these chalcogen elements: sulfur, selenium, or tellurium. Some recently developed chalcogenide glass fibers are As_2S_3 , As_2Se_3 , As_2Te_3 , and $\text{Ge}_{20}\text{Se}_{80}$ with core refractive indices of 2.35, 2.7, 3.5, and 2.35 respectively. These glass fibers are promising for the development of optical devices because of their high nonlinearity, chemical durability, and ability to transmit light in a wide spectral range (0.6 to 15 μm) with low losses [1].

The application of silica fiber for chemical sensing based on evanescent wave coupling phenomena is a well established technique. However, most of the chemical compounds have characteristic vibrational frequencies in the mid-IR wavelength region where silica fiber has very high attenuation. A chalcogenide glass fiber was used in infrared evanescent absorption spectroscopy to detect toxic chemicals (e.g. chlorinated hydrocarbons and benzene at lower concentrations) using a laser in the 3-12 μm wavelength range. It was found that a chalcogenide glass fiber with an acrylic coating could be used for detection of these chemicals with a high sensitivity [2]. It was also reported that a chalcogenide fiber based on sulfur (As_2S_3) with a Teflon cladding could be used as a temperature sensor [3]. However, applications of chalcogenide glass fiber (As_2Se_3) as a temperature sensor is limited due to its low melting point ($\sim 370^\circ\text{C}$) [4].

Recently, nonlinear optical switching phenomenon has been demonstrated in As_2Se_3 fiber using long period gratings created by acoustic waves. The switching was observed at pulse powers of 50W which is substantially lower than those observed for silica fibers which required kilowatt pulse powers [5]. Further, Z. Zhang et al. theoretically presented a new buffering technique in high speed optical networks based on Stimulated Brillouin Scattering (SBS) in As_2Se_3 fiber to delay the optical signal by many nanoseconds with little signal loss [6].

In this chapter we describe the fundamental properties of the arsenic selenium glass fiber and the application of it to develop a Brillouin fiber laser. A high power fiber laser which was developed in-house, presented in Chapter 2, was used as the pump for the Brillouin laser. The stability of the laser wavelength has been explored in relation to the input pump power level.

4.2 Arsenic Selenium Fiber (As_2Se_3)

Arsenic selenium glass has a layered two dimensional network consisting of structural units of a trigonal pyramid shape [4]. Arsenic Selenium has a wide transmission band from 0.8 to 12 μm with low loss [1;4], Figure 4.1 shows the loss spectrum of the fiber as given by the manufacture, CorActive, Canada. The fiber has a core refractive index of ~ 2.7 and a transmission loss of $\sim 1\text{dB/m}$ for radiation between 2 to 8 μm . The large absorption peak observed near 4.55 μm is attributed to the stretching vibration of the H-Se bond [7]. This fiber has a loss near 0.8dB/m in the telecom wavelength band.

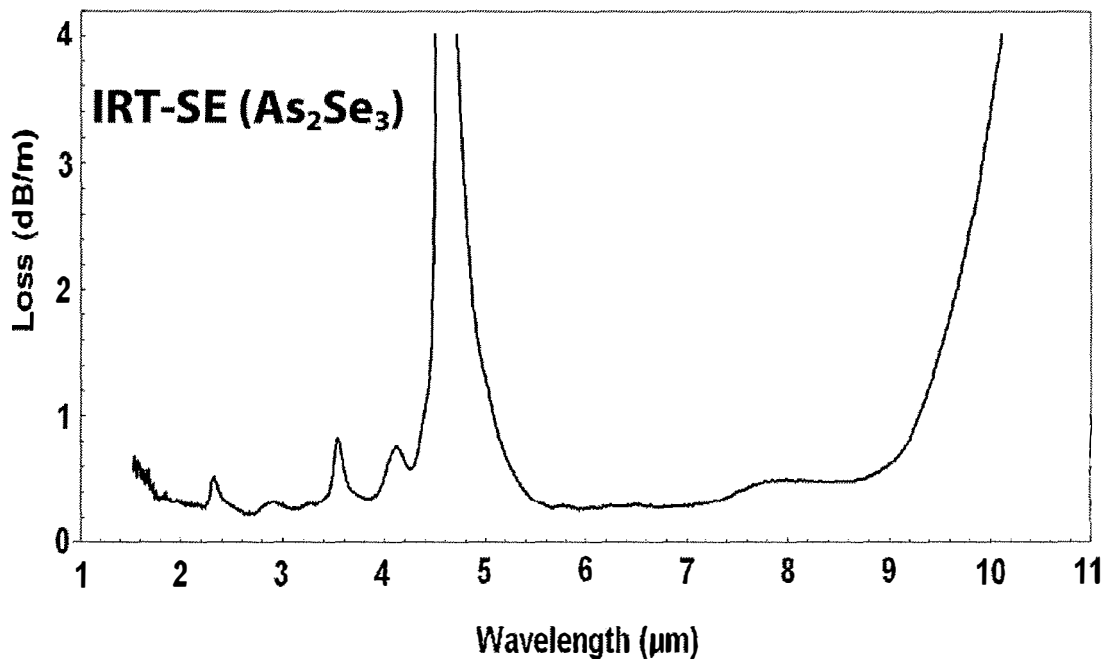


Figure 4.1: Loss spectrum of the arsenic selenium fiber used (CorActive).

As_2Se_3 fiber has large Raman and Brillouin gain coefficients compared to those of regular silica optical fiber. An optical device developed using silica glass fiber requires

longer lengths (~100s of meter) compared to chalcogenide glass fiber because of its lower nonlinearity. Chalcogenide fiber has many benefits over regular silica fiber, but also has its disadvantages. Compared to silica and other fibers chalcogenide fiber is fairly fragile. The fiber is very soft, delicate, and can easily break if not handled properly. The fiber has a very low melting point (~370°C) and thus, is very difficult to splice to a silica fiber which has a very high melting point (~1800°C). Another disadvantage of As₂Se₃ fibers is its tendency to allow light waves to propagate in the cladding, because of the high refractive indices of the glass slight amounts of bending will allow light from the core to transfer into the cladding where it will continue to propagate, reducing the power confined to the core. However, an application of a metal coating near the input and output ends of the fiber can reduce the radiation propagating in the cladding [8].

As described in Chapter 1 (Section 1.4.1), Stimulated Brillouin Scattering occurs when an acoustic wave is formed through electrostriction in a fiber and reflects the incident pump power at a shifted wavelength. Stimulated Brillouin Scattering (SBS) is much easier to achieve and maintain in As₂Se₃ than SiO₂ fiber, this is due to the longer phonon lifetime of 12 ns, at 1550 nm, in arsenic selenium fiber compared to the phonon lifetime of 5 ns, at 1550nm, in silica fiber [6]. Further, the decay rate is equal to the inverse of the phonon lifetime and the Brillouin linewidth (table 4.1) is directly proportional with the inverse phonon lifetime. The Brillouin gain coefficient of As₂Se₃ glass fiber was found to be around 6.2×10^{-9} m/W [9] this is about 124 times larger than that of SiO₂, which is approximately 5×10^{-11} m/W [10;11].

Brillouin Parameters

Acoustic Phonon Decay Rate: $\Gamma_B = \frac{1}{\tau_B}$

where τ_B is the acoustic phonon lifetime.

Brillouin Linewidth: $\Delta \nu_B = \frac{\Gamma_B}{2\pi}$

Brillouin Shift: $\nu_B = \frac{2n v_a}{\lambda_p}$

where v_a is the speed of sound in the medium.

Brillouin Gain Coefficient: $g_B = \frac{2\pi n^7 p_{12}^2}{c \lambda_p^2 \rho v_a \Delta \nu_B}$

where p_{12} is the longitudinal photoelastic constant of the material and ρ is the density of the material.

Brillouin Pump Threshold: $P^{cr} \cong \frac{21 A_{eff}}{g_B L_{eff}} \quad [10]$

Where A_{eff} is the effective core area and L_{eff} is the effective length

Empirical Formula	SiO₂	As₂Se₃
Melting Point(°C)	1800 ⁱ	370 ^a
Index of Refraction	1.47 ^b	2.7 ^k -2.81 ^b
Velocity of Light (m/s)	$\sim 2 \times 10^8$ Calc.	$\sim 1 \times 10^8$ Calc.
Loss (dB/m) (at ~ 1560 nm)	0.001 ^b	0.9 ^b
Transmission Range (μ m)	1 - 2 ^h	0.8 - 12 ^c
Speed of Sound (m/s)	5960 ^d	2258 ^e
Nonlinear Index Coefficient (m ² /W)	2.6×10^{-20} f	1.1×10^{-17} f
Phonon Lifetime (ns)	5 ^e	12 ^e
Brillouin Shift (GHz)	11.3 Calc.	8.2 Calc.
Brillouin Gain Coefficient (m/W)	5×10^{-11} g	6.2×10^{-9} d

(^{Calc.} Calculated, ^a Ref.[4], ^b Ref.[12], ^c Ref.[1], ^d Ref.[9], ^e Ref.[6], ^f Ref.[13], ^g Ref.[10], ^h Ref.[14], ^j Ref.[15], ^k Ref.[1])

Table 4.1: Important parameters of As₂Se₃ and SiO₂.

Calculations for SiO₂

$$\text{Velocity in Fiber: } v = \frac{\text{velocity of light}}{\text{index of refraction}} = \frac{c}{n} = \frac{3 \times 10^8}{1.47} \approx 2 \times 10^8 \text{ m/s}$$

$$\text{Brillouin Shift: } v_B = \frac{2nv_a}{\lambda_p} = \frac{2 \times 1.47 \times 5960}{1550 \times 10^{-9}} = 11.3 \text{ GHz}$$

Similarly, the speed of light and Brillouin shift in chalcogenide glass fiber are calculated to be 1.1×10^8 m/s and ~ 7.9 GHz, respectively.

4.3 Experimental Setup and Discussions

We encountered several challenges after we started using the nonlinear chalcogenide fiber, because the fiber has completely different physical characteristics than regular silica fiber, it was not possible for us to splice the As_2Se_3 fiber into the laser cavity. This is due to the fact that As_2Se_3 glass has a melting point around 370°C which is almost 5 times less than that of the silica based optical fiber, which is $\sim 1800^\circ\text{C}$ [15]. We resolved this issue by using a free space coupling method to couple light into and out of the nonlinear fiber.

Before making any free space connection we had to prepare the ends of the As_2Se_3 fiber. As suggested by CorActive, we soaked the fiber in dichloromethane to soften the jacket before using jacket strippers to remove it from the glass fiber. Another method of removing the protective jacket from the delicate As_2Se_3 is to use a solution dubbed Nano-StripTM [8]. The fiber was cleaved with a cleaver at a low tension setting (~ 80 psi), which reduces the damage to the fiber. The fiber ends were cleaved flat, which is essential for good coupling efficiency, with occasional chipping around the outside edge but did not affect the performance of the fiber. A tapered single-mode fiber with an anti-reflection coating was used for free space coupling into the As_2Se_3 . The choice to use a tapered fiber was made after performing several experiments using a straight cleaved fiber, a ball lensed fiber, and the tapered fiber. It was found that the tapered fiber allowed

the most radiation to be coupled into and out of the As₂Se₃ fiber. Free space coupling can introduce very high insertion loss due to the Fresnel reflection from the air-core interface; numerical aperture (NA) or core mismatching; lateral, longitudinal, or angular misalignment. The following paragraphs will explain these losses in more detail as well as the methods we used to address or, if possible, eliminate them.

Fresnel reflection occurs at any boundary where a change in refractive index occurs and is more substantial for higher refractive index. The percentage of reflected light is given by:

$$Reflection = \left(\frac{n_1 - n_2}{n_1 + n_2} \right)^2 \quad (4.1)$$

The As₂Se₃ fiber has a high core refractive index, which resulted in a reflection of approximately 21% of the incident power. The reflection loss could be reduced substantially with an anti-reflection coating.

Losses due to differences in numerical aperture only occur when transmitting light to a fiber with a lower NA. This loss is determined in dB by the following equation:

$$\eta_{NA} = \log \left[\left(\frac{NA_2}{NA_1} \right)^2 \right] \quad (4.2)$$

The NA of the As₂Se₃ fiber is 0.19, which is larger than the numerical aperture of the silica fiber, ~0.11. The loss from this is about 0.47dB.

Losses due to mismatches in core diameter occur when light is being coupled from a larger core to a smaller core.

$$Loss_{core} = \log \left[\left(\frac{d_2}{d_1} \right)^2 \right] \quad (4.3)$$

The loss due to core mismatching was minimal since the mode field diameter of the selected tapered fiber is $\sim 5 \mu\text{m}$ and the core diameter of the As_2Se_3 was $5.1 \mu\text{m}$.

Another problem associated with free space coupling is aligning the end faces of the two coupling fibers. If the fibers are not aligned properly, losses due to longitudinal, axial or angular misalignment can be detrimental to the coupling efficiency. Longitudinal offsetting (Figure 4.2a) occurs when the cores of the fibers are on the same axis but the distance between the two end faces is too large. This can allow the majority of emitted radiation to couple into the cladding, instead of the core, where it will be lost. Axial misalignment (Figure 4.2b) occurs when the cores of the fiber are not on the same axis. This results in some or all of the power being coupled into the cladding of the fiber. In angular misalignment (Figure 4.2c) the fiber ends are not parallel with one another.

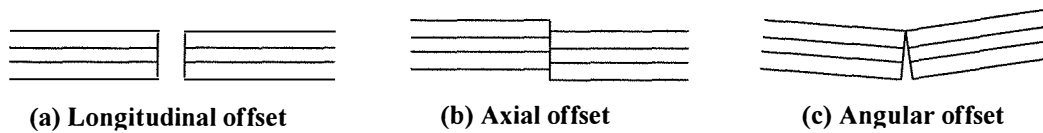


Figure 4.2: Different misalignments that can occur when coupling fibers through free space techniques.

We mounted both the lensed fiber and chalcogenide fiber on 3-axis translation stages, with a resolution of $1 \mu\text{m}$ and 1nm , respectively. We were able to obtain maximum power coupling after making adjustments to the translation stages.

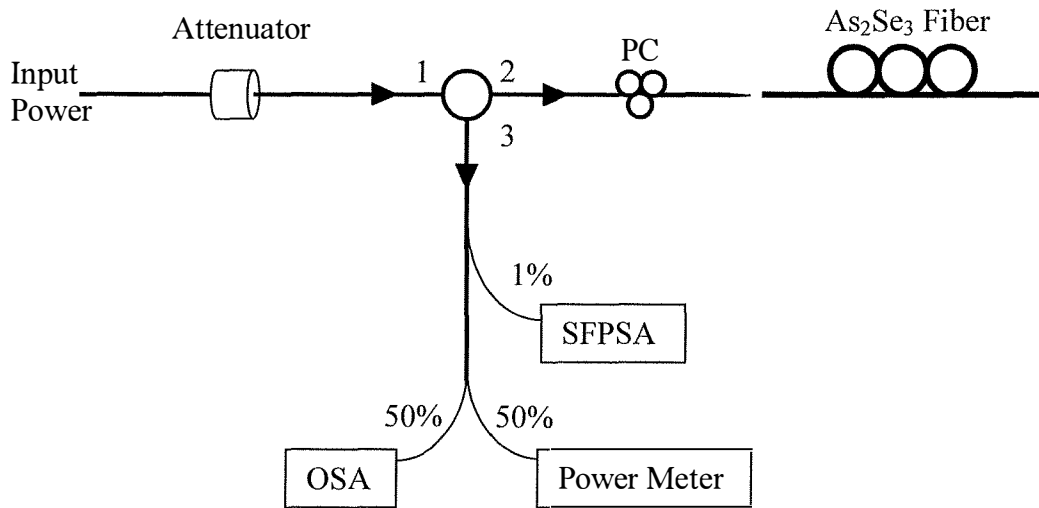


Figure 4.3: The circuit diagram of the Brillouin fiber laser.

A diagram of the resonator for the Brillouin fiber laser based on the nonlinear chalcogenide fiber in a Fabry-Perot cavity configuration is presented in Figure 4.3. The pump radiation enters the system from port 1 of a polarization independent optical circulator. The radiation was then emitted out of port 2 of the optical circulator which is spliced to a polarization controller. This polarization controller controls the polarization of the light entering the nonlinear and lensed fiber. The tapered fiber, which was spliced to the end of the polarization controller, was placed on a three axis translation stage to couple the light into and out of the chalcogenide fiber. The Brillouin scattered light, travels back through the PC, enters port 2 and was directed towards port 3. To monitor the output of the laser we coupled out 1% of the power to our Scanning Fabry-Perot Spectrum Analyzer (SFPSA), and then the remaining power was split (50:50) to a power meter and Optical Spectrum Analyzer (OSA).

4.4 Results and Analysis

We experimented with fiber ends that were flat cleaved, ball lensed, and tapered for coupling radiation from the laser into the chalcogenide fiber. We found that the flat cleaved fiber, with a core diameter of 8 μm gathered the radiation fairly well; however, the insertion loss was high due to the core diameter mismatch with smaller core diameter (5.1 μm) of the As_2Se_3 fiber. The ball lensed fiber was found to be good for gathering the backscattered light but did not transmit the light adequately enough. After a series of experiments we determined that the tapered fiber was the best candidate for coupling. This is because the spot size diameter of the tapered fiber was 5 μm which matches with the core diameter (5.1 μm) of the chalcogenide fiber and resulted in a higher coupling efficiency. The tapered fiber had a working distance of 26 μm and was adjusted by using the translation stages.

It was also found that the chalcogenide fiber started melting at high input power (~ 500 mW) when we brought the tapered fiber very close or tried to adjust the coupling efficiency by moving the XYZ stage while the laser was operating. This could be due to the high power propagating into the cladding and eventually leaking into the jacket which is made of a polymer material.

The laser described in Chapter 2 was used as the pump for the Brillouin fiber laser. Since the wavelength of the Brillouin laser was very close to the wavelength of the pump laser, the stability of the pump laser was extremely important to observe Brillouin lasing. To control the input power into the Brillouin fiber laser cavity an attenuator was inserted before Port 1 of the circulator (Figure 4.3). We obtained the maximum coupling efficiency of the tapered fiber and chalcogenide fiber by using a low input pump power

and adjusting the X, Y, and Z axes of the translation stages. Figure 4.4 shows the variation of the output power from the chalcogenide fiber with the X axis position of the translation stage at an optimum location for the Y and Z axes. The input pump power to the Brillouin fiber laser cavity was increased after optimizing the location of the two fibers. There was no damage to the fiber end at high power, which also confirmed maximum coupling of pump power into the core of chalcogenide fiber.

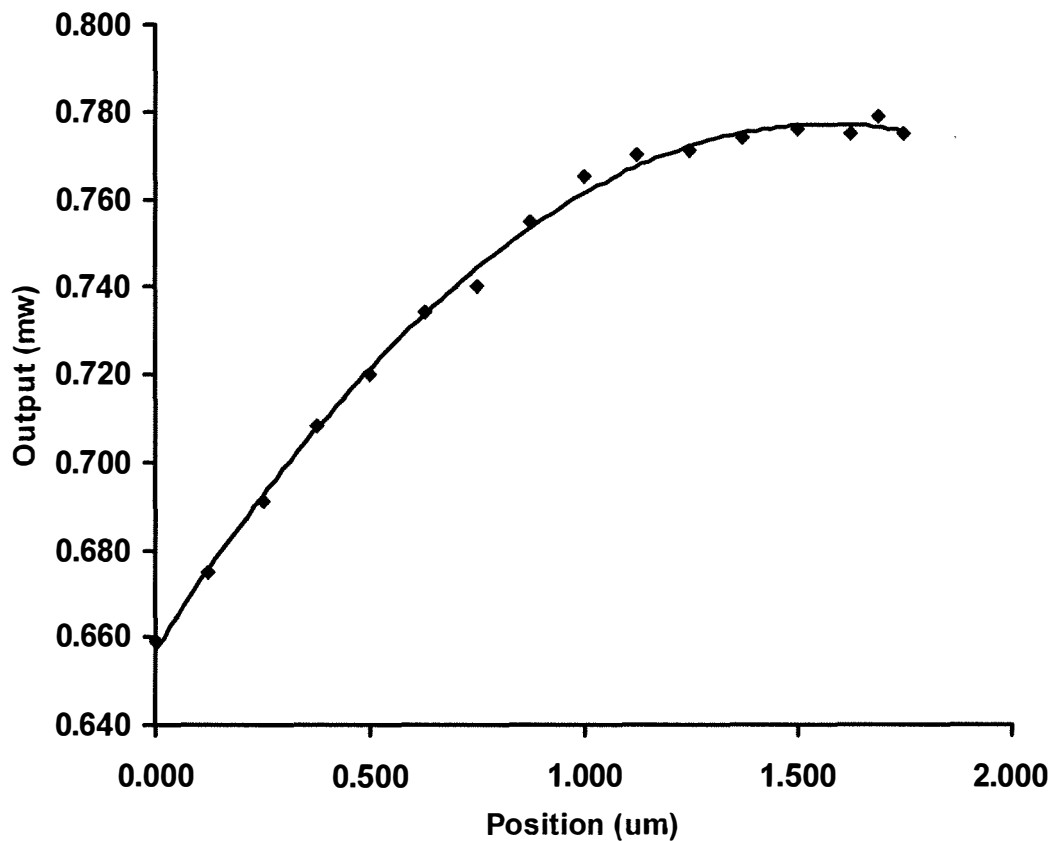


Figure 4.4: X-position versus output power from the chalcogenide fiber for an input pump power of 1.18 mW.

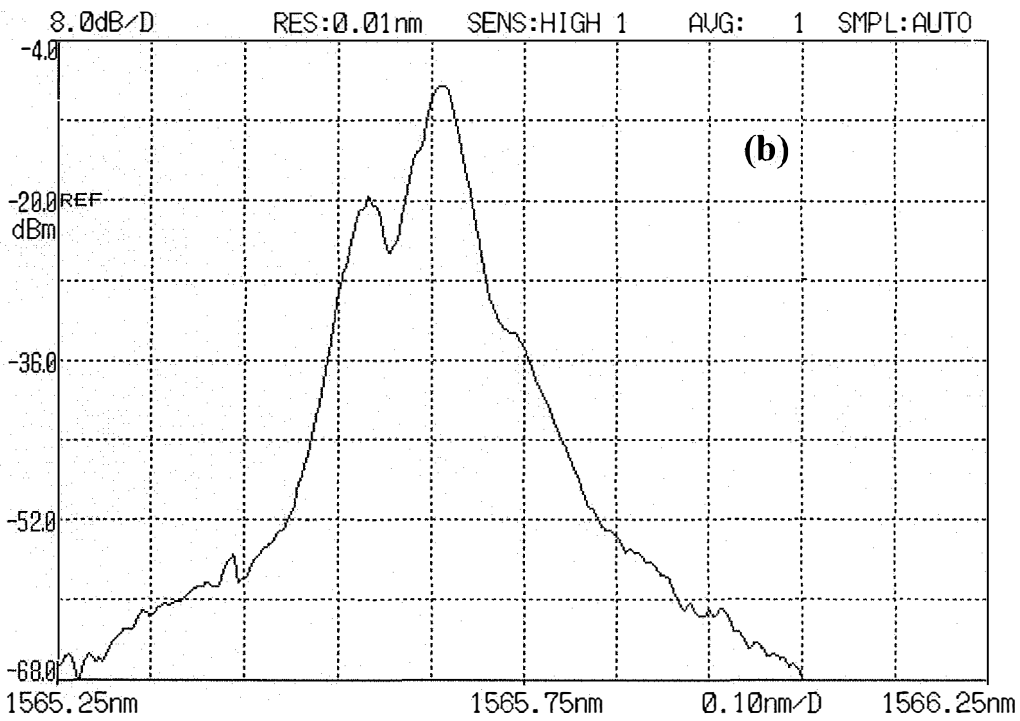
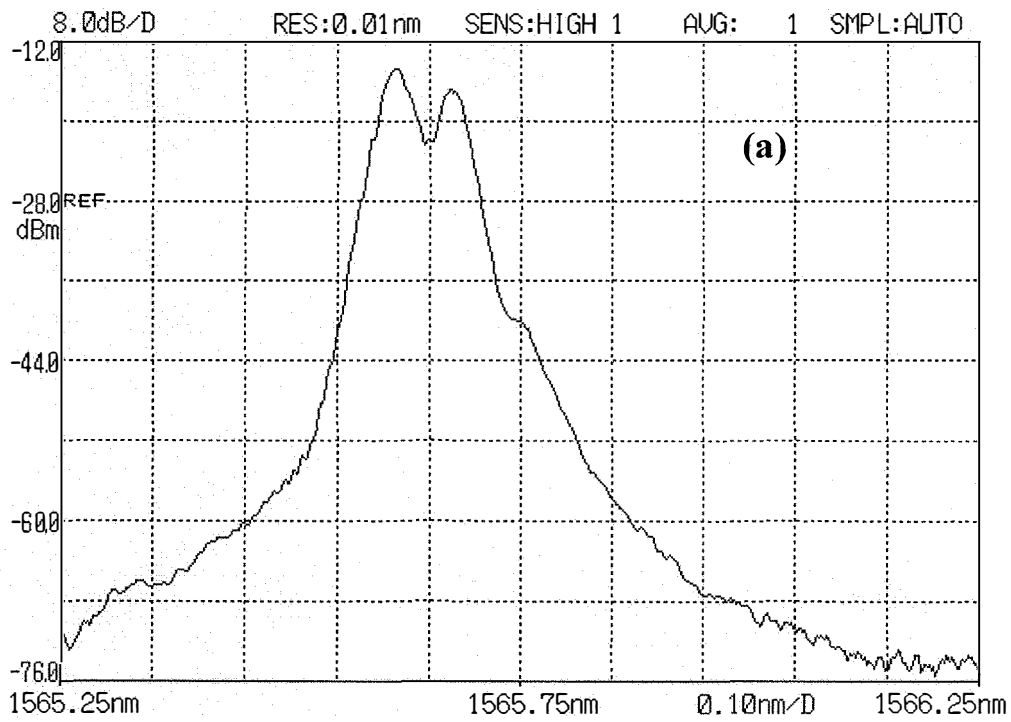


Figure 4.5: Output obtained from optical spectral analyzer at different input powers with a pump wavelength of 1565.60nm: (a) 1.5 A (124mW) and (b) 3.0A (300 mW).

Figure 4.5 shows the output of the Brillouin fiber laser obtained using the Optical Spectrum Analyzer (OSA). We used a 1.7m length of chalcogenide fiber for this experiment. The effective length of the chalcogenide glass fiber was ~ 0.88 m. We found that our results closely resembled those reported by I. D. Aggarwal et al [16]. The second peak on the right hand side in Figures 4.5(a) and 4.5(b) corresponds to the Brillouin laser wavelength. The output of the laser contains a fraction of pump power due to Fresnel reflection from the flat end of the chalcogenide fiber. Since the linewidth (~ 0.000112 nm or 14 MHz) of the pump laser was very small compared to the resolution of the OSA (0.01 nm), it was difficult to separate the pump and the Brillouin laser wavelength with our spectrum analyzer. The threshold power for the Brillouin laser was high compared to the results published by others researchers; this is due to the large laser linewidth and shorter length of the Brillouin gain medium.

In order to assure that SBS was present we also monitored the output of the laser using SFPSA. At low power the output of the laser was due to the reflected light at the front face of the chalcogenide glass fiber and was single mode with no mode hopping. As we increased the input pump power (but remained below 300 mW where the laser is single-mode) two or more modes were visible on the SFPSA, which confirmed the presence of the Brillouin laser wavelength. It was difficult to measure the separation between two modes due to the instability of the laser wavelengths, which we attributed to the fluctuation of environmental parameters such as temperature.

The linewidth of the incident and back scattered light was measured using the SFPSA. It was found that for a laser with a linewidth of ~ 17 MHz, at an input of 2.1A, the linewidth reduced to ~ 11 MHz after being backscattered from the nonlinear fiber.

The reduction of laser linewidth is known as nonlinear line narrowing, and was due to the stimulated Brillouin scattering.

4.5 Discussion and Summary

The Brillouin fiber laser described in this section was based on the pump laser we had developed and reported in Chapter 2. A short length of highly nonlinear chalcogenide glass fiber was used to develop the nonlinear laser. The output obtained from our experiments exactly matches with the previously reported results [16]. The coupling efficiency of the pump power to the chalcogenide glass fiber was improved by introducing a tapered single-mode glass fiber.

The pump laser we had developed will be a good candidate for developing photonic devices based on nonlinear optical phenomenon. Further, by introducing a temperature stabilization scheme, we would be able to improve the stability of the laser.

References

- [1] D. Lezal, J. Pedlikova, and J. Zavadil, "Chalcogenide glasses for optical and photonics applications," *Journal of Optoelectronics and Advanced Materials*, vol. 6, no. 1, pp. 133-137, Mar.2004.
- [2] J. S. Sanghera, F. H. Kung, L. E. Busse, P. C. Pureza, and I. D. Aggarwal, "Infrared Evanescent Absorption-Spectroscopy of Toxic-Chemicals Using Chalcogenide Class Fibers," *Journal of the American Ceramic Society*, vol. 78, no. 8, pp. 2198-2202, Aug.1995.
- [3] J. S. Sanghera and I. D. Aggarwal, "Active and passive chalcogenide glass optical fibers for IR applications: a review," *Journal of Non-Crystalline Solids*, vol. 257, pp. 6-16, Oct.1999.
- [4] G. E. Snopatin, V. S. Shiryaev, V. G. Plotnichenko, E. M. Dianov, and M. F. Churbanov, "High-purity chalcogenide glasses for fiber optics," *Inorganic Materials*, vol. 45, no. 13, pp. 1439-1460, Dec.2009.
- [5] H. C. Nguyen, D. I. Yeom, E. C. Magi, L. B. Fu, B. T. Kuhlmeier, C. M. de Sterke, and B. J. Eggleton, "Nonlinear long-period gratings in As₂Se₃ chalcogenide fiber for all-optical switching," *Applied Physics Letters*, vol. 92, no. 10 Mar.2008.
- [6] Z. Y. Zhang, X. J. Zhou, R. Liang, Z. J. Qin, and Y. Liu, "Numerical investigation on buffer performance based on acoustic excitation by stimulated Brillouin scattering in an As₂Se₃ fiber," *Optics Communications*, vol. 282, no. 14, pp. 2746-2751, July2009.
- [7] V. Q. Nguyen, J. S. Sanghera, P. C. Pureza, and I. D. Aggarwal, "Effect of heating on the optical loss in the As-Se glass fiber," *Journal of Lightwave Technology*, vol. 21, no. 1, pp. 122-126, Jan.2003.
- [8] K. Krishnaswami, H. Qiao, B. E. Bernacki, and N. C. Anheier, "Characterization of Single-mode Chalcogenide Optical Fiber for Mid-Infrared Applications," 7325 ed 2009, pp. 73250Z-73250Z-10.
- [9] K. S. Abedin, "Observation of strong stimulated Brillouin scattering in single-mode As₂Se₃ chalcogenide fiber," *Optics Express*, vol. 13, no. 25, pp. 10266-10271, Dec.2005.
- [10] G. P. Agrawal, *Nonlinear Fiber Optics*, 3rd ed Academic Press, 2001.
- [11] G. W. Faris, L. E. Jusinski, and A. P. Hickman, "High-Resolution Stimulated Brillouin Gain Spectroscopy in Glasses and Crystals," *Journal of the Optical Society of America B-Optical Physics*, vol. 10, no. 4, pp. 587-599, Apr.1993.
- [12] J. S. Sanghera, C. M. Florea, L. B. Shaw, P. Pureza, V. Q. Nguyen, M. Bashkansky, Z. Dutton, and I. D. Aggarwal, "Non-linear properties of chalcogenide glasses and fibers," *Journal of Non-Crystalline Solids*, vol. 354, no. 2-9, pp. 462-467, Jan.2008.
- [13] R. E. Slusher, G. Lenz, J. Hodelin, J. Sanghera, L. B. Shaw, and I. D. Aggarwal, "Large Raman gain and nonlinear phase shifts in high-purity As₂Se₃ chalcogenide fibers," *Journal of the Optical Society of America B-Optical Physics*, vol. 21, no. 6, pp. 1146-1155, June2004.
- [14] J. S. Sanghera, L. B. Shaw, and I. D. Aggarwal, "Chalcogenide Glass-Fiber-Based Mid-IR Sources and Applications," *Ieee Journal of Selected Topics in Quantum Electronics*, vol. 15, no. 1, pp. 114-119, Jan.2009.

- [15] A. H. Rose, "Devitrification in annealed optical fiber," *Journal of Lightwave Technology*, vol. 15, no. 5, pp. 808-814, May 1997.
- [16] C. Florea, M. Bashkansky, Z. Dutton, J. Sanghera, P. Pureza, and I. Aggarwal, "Stimulated Brillouin scattering in single-mode As₂S₃ and As₂Se₃ chalcogenide fibers," *Optics Express*, vol. 14, no. 25, pp. 12063-12070, Dec. 2006.

Future work

We presented a tunable continuous wave single-longitudinal mode fiber laser. This laser can operate in either CW or PULSED regime. The laser can be utilized for the following applications:

1. Supercontinuum generation using a fiber with high nonlinearity.
2. Slow light generation.
3. Developing Raman Laser

